UNIVERSITY OF CALIFORNIA,
IRVINE

# Optimal Conditions for a Cryptochrome Based Magnetic Compass

DISSERTATION

submitted in partial satisfaction of the requirements
for the degree of

DOCTOR OF PHILOSOPHY

in Physics

by

Shawn Strausser

Dissertation Committee:
Professor Thorsten Ritz, Chair
Associate Professor Jun Allard
Professor Zuzanna Siwy

2022

# TABLE OF CONTENTS

# LIST OF FIGURES

# ACKNOWLEDGMENTS

This work has been supported by the Air Force Office of Scientific Research award No. FA9550-14-1-0409.

# VITA

## Shawn Strausser

### EDUCATION

**Doctor of Philosophy in Physics** **2022**
University of California-Irvine *Irvine, California*

**Bachelor of Science in Physics** **2014**
University of Michigan, Dearborn *Dearborn, Michigan*

### RESEARCH EXPERIENCE

**Graduate Research Assistant** **2016-2022**
University of California, Irvine *Irvine, California*

### TEACHING EXPERIENCE

**Teaching Assistant** **2014–2017**
University of California, Irvine *Irvine, California*

# ABSTRACT OF THE DISSERTATION

Optimal Conditions for a Cryptochrome Based Magnetic Compass

By

Shawn Strausser

Doctor of Philosophy in Physics

University of California, Irvine, 2022

Professor Thorsten Ritz, Chair

European robins can detect the direction of the Earth's magnetic field, forming an internal compass which aids them in migration and other navigational tasks. The physical basis of this magnetic sense arises from a light-initiated chemical reaction which proceeds through a magnetically sensitive radical-pair intermediate. The pathway of this reaction is sensitive to Earth strength fields, with the products encoding directional information. The photoreceptor cryptochrome has been suggested as a magnetic receptor, owing to its ability to form radical pairs in response to light absorption. However, numerous challenges remain in establishing cryptochrome as the molecular basis of magnetoreception.

Thermal noise causes the positions of the radicals to fluctuate, affecting the magnetic environment and therefore the reaction pathway. Using model calculations, we show that a magnetic compass based on cryptochrome is robust to thermal fluctuations, and that its performance improves, becoming more robust to other sources of noise.

Motivated by this result we investigate the limits of its performance by determining the optimal radical pairs. Using a genetic based algorithm we show: (1) the simplest radical-pair system possible exhibits a high degree of sensitivity and (2) the radical pair formed on cryptochrome is nearly optimal.

Since the magnetic compass is light-dependent, it has been challenging to understand how night-migration is possible, given the low-light conditions. Furthermore, behavioral experiments have demonstrated that if the light intensity is too high or low (i.e. exhibits a functional window), the magnetic compass no longer works. Using a suggested photocycle for cryptochrome we show: (1) a magnetic compass based on cryptochrome performs better under low-light conditions and (2) the functional window can be understood as a consequence of its photocycle.

Another challenge facing cryptochrome is establishing which reaction step is magnetically sensitive. Two reactions have been proposed – the forward light-dependent step and the 'dark' backward reaction. Combining cryptochrome's photocycle with a phosphorylation binding model, we present calculations in alternating light and magnetic conditions which support the dark reaction as being magnetically sensitive.

# Chapter 1

# Introduction

Diverse organisms including European Robins and *Arabidopsis Thaliana* can detect the Earth's magnetic field to drive key biological processes, e.g., compass orientation in European Robins [154, 110] and growth and development in *Arabidopsis Thaliana*. [2, 1, 19] The basis for this so-called 'magnetoreception' has been suggested to originate from a chemical reaction proceeding through magnetically-sensitive radical-pair intermediates whose reaction pathway (i.e. products) depends on the strength and/or orientation of an external magnetic field, thereby encoding directional information into its reaction products. [116] This has been suggested to form the physical basis of biological magnetic compasses, in particular that of the European robin. [117] The protein cryptochrome has been suggested as the magnetoreceptor, in part, due to it ability to form radical-pairs upon light-absorption. [110]

This thesis is concerned with three broad questions: (1) what is the effect of noise on the avian magnetic compass, (2) what are the limits to its performance, and (3) what are the effects of light-intensity on cryptochrome's photocycle and signal transduction. For the first question it is found that noise in some instances can improve the compass, while also allowing it to function for shorter radical-pair lifetimes. In the second, we use model systems to investigate

the optimal nuclear environments where it is found that the simplest conceivable radical-pair can produce a directional yield that displays a needle-like feature, thereby providing a 'precise' compass. In addition, it is found that the radical-pair based on cryptochrome possess a nuclear structure that performs near its limits. Finally, in the third case we provide support for cryptochrome as the magnetoreceptor by showing: (1) its signaling state displays a biphasic response to light-intensity, consistent with experimental observations of avian orientation, [159] and (2) the maximal response of this signalling state increases for lower-light intensities, suggesting that it performs better under low-light conditions, consistent with the observation that many birds migrate at night. [41, 82]

In this chapter we provide a brief overview of the literature with a focus on the experimentally determined characteristics of the avian magnetic compass relevant for this thesis. We then discuss the experimental results that supports the radical-pair mechanism as the basis of magnetoreception, and how it could be realized in a biological system using cryptochrome. Finally, we give an outline of the thesis.

## 1.1 Background

Birds utilize a variety of cues [148] to navigate during migration, including the sun, [60] celestial patterns, [26, 27], landmarks, and crucially, Earth's magnetic field. [152] Use of a magnetic compass had been speculated before its discovery due to the need of having a compass that works in all environmental conditions, particularly during overcast night-migration which precludes the use of the others. [26] Research on these compasses is typically done at the behavioral level [85, 99, 159] – during spring migration, e.g., birds experience a strong drive to fly north. This behavior is innate (i.e. not learned), persistent, and can be induced in laboratory settings by changing the length of day, thereby making it a reliable source of experimental study. Furthermore, this behavior persists even when placed inside a

cage, so that by measuring their (average) orientation, researchers can determine how their orientation will respond to changes in external stimuli.

To test whether birds possess a magnetic compass, European robins are placed in a cage during migratory season, in the absence of any other cues. Under the local geomagnetic field, they will tend to orient in their seasonally appropriate migratory direction, e.g., north in the spring. Rotating the magnetic field they experience so that magnetic-north is rotated, the birds correspondingly changed their direction of flight, indicating that they can detect and respond to changes in the magnetic field. [152] Furthermore, it was discovered the mechanism responsible is unlike a magnetic compass based on a needle – when the horizontal (or vertical) component of the field was reversed, the birds reversed their direction of orientation. However, when both components were reversed, so that the field was inverted, the birds oriented as they would under the original magnetic field – i.e., they are insensitive to an inversion of the field. [154] In contrast, a handheld magnetic compass will not change its orientation when the vertical component is flipped, and will reverse directions when the field is inverted. Furthermore, when the inclination was equal to zero, the birds became disoriented, further indicating they detect the inclination of the field and not the polarity. These properties characterize the avian magnetic compass as 'inclination-based'. Finally, instead of distinguishing between north and south, birds distinguish between 'poleward' and 'equatorward', with help from the direction of gravity. [154]

However, in order to *navigate* to a location beyond direct sensory perception, both a compass *and* a 'map' are required. In addition to providing the basis for a compass, the Earth's magnetic field also provides information that can form the basis of a 'map'. Its inclination and strength varies predictably over latitude, which has been suggested to provide a coordinate system. [108] Magnetic maps can be used for a variety of purposes, e.g., from changing migratory direction at an appropriate location [74, 90] to navigating toward a specific home area. [75] Furthermore, it has been shown that sea-turtles when exposed to a magnetic

field encountered on its migration changes its orientation accordingly. In other words, this specific combination of orientation and field-strength act as a 'sign-post', signalling the turtle to change its course.

However, in order to *navigate* to a location beyond direct sensory perception, both a compass *and* a 'map' are required. Magnetic maps can be used for a variety of purposes, e.g., from changing migratory direction at an appropriate location [74, 90] to navigating toward a specific home area. [75] Furthermore, it has been shown that sea-turtles when exposed to a magnetic field encountered on its migration changes its orientation accordingly. In other words, this specific combination of orientation and field-strength act as a 'sign-post', signalling the turtle to change its course. Information from the geomagnetic field, i.e., its inclination and magnitude, can form the basis of numerous biological functions, including a map. In addition to providing a magnetic compass, which aids in behaviors like migration and homing, it can also be used to derive geographic position. [76] The magnetic inclination and strength varies predictably over latitude, which has been suggested to provide a coordinate system. [108]

An initial suggested mechanism for *how* birds can detect the Earth's magnetic field relied on light, [66] thereby prompting experiments to determine if there are any effects of light. [155] It was discovered that light is necessary to observe migratory orientation, i.e., birds become disoriented in *complete* darkness. [66, 155, 125] Numerous follow up studies have demonstrated a bewildering array of responses to various light conditions [153, 85, 157, 151, 159, 92, 150]. In particular, it has been shown that the spectral character of the light-source is relevant – studies using monochromatic light sources in orientation studies have demonstrated short-wavelength light (i.e. approximately 300 – 565 nm) is required for proper orientation, with a sharp cutoff at approximately 565nm. Additionally, it has been shown that light-intensity within some 'functional window' is required, i.e., intensities that are too high or low lead to behavioral responses different from the expected migratory orientation,

indicating that their magnetic compass is not functioning. [158] These features appear to be preserved across various species, suggesting the same underlying mechanism in each of them. [144]

Taken together, these experiments suggest the mechanism responsible must be inclination-based and light-dependent. So far, the only magnetoreception mechanism that has been characterized definitively is in so-called 'magnetotactic bacteria'. These bacteria are characterized by specialized organelles containing chains of magnetite (iron-oxide nanoparticles) that impart to it a permanent magnetic moment, thereby exerting a torque and aligning it (passively) with the Earth's magnetic field, enabling them to more easily find their preferred oxygen environment. [13] However, it is not expected that a magnetite based compass [57] operates in birds, as it is not inclination based or light-dependent. However, it has been suggested to play a role in other magnetoreceptive functions, namely as the basis of a map. [156] Furthermore, it is possible that both magnetoreceptive systems can coexist, with one providing the basis for a 'map' (e.g. magnetite), [138, 88] and another the basis of a compass (e.g. the radical pair mechanism) – both of which are required for navigation. [73, 146, 99] Although a magnetic compass has been discovered elsewhere, e.g. mole rats [56], newts [99] and *Drosophila Melanogaster*, [30] birds have remained the model organism to study magnetoreception, in part due to the clear function of magnetoreception in migration, and difficulties with similar systems. [98]

Numerous other mechanisms beyond magnetite have been proposed, [66, 128, 116] namely, a light-initiated chemical reaction involving magnetically-sensitive radical-pair intermediate whose reaction pathway can be affected by the orientation of an external magnetic field, thereby encoding directional information into a biochemical signal. [116] That is, by changing the orientation of the external field, the products formed can be predictably changed. If these products are biologically active, i.e., capable of initiating a signal transduction pathway, it would then form the basis of a magnetoreception sensory system. In principle, radical-

pairs can be formed through light-independent means, e.g. homolytic bond cleavage, so that the radical-pair mechanism does not *require* light. Indeed, there has been recent evidence which suggests a light-independent reaction step in cryptochrome as being the magnetically sensitive step. [142] Support for the radical-pair mechanism as the basis of magnetoreception includes: (1) it is inclination based and displays the proper symmetry, (2) is light-dependent; in particular, radical-pairs are often formed between molecules through light-induced electron transfer, and (3) is sensitive to extremely weak magnetic fields, i.e., Earth's, and (4) radiofrequency magnetic fields have been shown to disrupt the avian magnetic compass, [112, 84, 123, 134, 145, 40, 67] consistent with a radical-pair based, but not magnetite, compass. [131, 161, 126] Indeed, any biochemical mechanism that responds to magnetic fields, especially weak ones, is notable as it is difficult to explain how fields less than one Tesla result in magnetic field effects. [127]

The above considerations suggest a photoreceptor whose photocycle involves a radical-pair, with both the light dependent and independent reactions being suggested to form magnetically sensitive radical-pairs. [142, 104] The wavelength dependence of orientation can be understood through the absorption spectrum of the photoreceptor, as wavelengths outside of this will not initiate the reaction. This suggests that it absorbs light with wavelengths ($\approx$ 300 – 565 nm), but not elsewhere. Numerous photoreceptor proteins satisfy this constraint, e.g., melanopsin and phototropins, however none of them are known to form radical-pairs, [110, 25, 33] except chlorophyll which does not exist in birds. These considerations led to the suggestion of cryptochrome, a short-wavelength photoreceptor protein as a candidate magnetoreceptor, [110] owing to its absorption spectrum which closely matches the wavelength dependence of avian orientation. Furthermore, it is highly homologous to its evolutionary precursor, photolyase, [115, 141] which is known to form radical-pairs upon light-absorption. The spectral properties of cryptochrome results from its bound chromophore, flavin, which forms a radical-pair with a nearby tryptophan amino-acid residue upon light-absorption, a necessary requirement to observe magnetic field effects. First discovered in plants, [1] cryp-

tochrome has subsequently been found in birds, particularly in their retina, [80, 84, 91, 93, 33] an ideal location for light-absorption. In addition, this location provides a number of ordered structures with which cryptochrome can anchor – to function as a directional compass, it is necessary that *some* degree of ordering is required, with theoretical calculations suggesting that significant fluctuations can be tolerated. [38, 65] In addition to their proposed role as a magnetoreceptor, cryptochromes also regulate a variety of other biological processes, including plant growth and development, as well as light-dependent (and independent) roles in circadian rhythms. [72, 62, 135, 32]

Cryptochromes along with photolyases form a 'protein superfamily', [1] characterized by a conserved N-terminal domain which binds the chromophore flavin. [71, 79, 19, 20] Indeed, cryptochromes are defined by their high structural similarity to photolyases, which in addition have acquired novel roles in signalling. Signalling of cryptochrome is typically done through its C-terminal domain; variability in this domain enables binding of different protein partners, thereby enabling a wide variety of signalling functions. [164, 169, 69] Subsequent to light-absorption an electron transfer occurs from a nearby tryptophan residue to flavin, [31, 167] forming a magnetically-sensitive radical-pair and leading to numerous structural changes [96] that expose its C-terminal domain, [139, 10, 15] enabling, e.g., phosphorylation [4, 119, 120, 86] which has been shown to correlate with its function and regulation. Other post-translational modifications can result, e.g., dimerization, binding of metabolites (e.g. ATP), and ubiquinitation. [106]

Numerous lines of evidence provide support for cryptochrome as a magnetoreceptor. In *Sylvia borin*, cryptochrome has been shown to form radical-pairs in response to blue-light absorption. [70, 12] Furthermore, the lifetime of this radical-pair was found to be on the order of milliseconds, i.e., sufficiently long to initiate signal transduction. In *Drosophila Melanogaster* cryptochrome, magnetic field effects have been observed in electron-transfer reactions, [121] albeit for millitesla field strengths, about three-orders of magnitude too small.

Photolyase from *Escherichia coli* was also found to be sensitive to magnetic fields, but again under millitesla fields. [36] However, such effects appear to be incidentally related to the flavin chromophore, and therefore sensitivity to Earth strength fields would be unexpected. In contrast, cryptochrome has likely underwent significant evolution to detect Earth strength magnetic fields. Similar experiments have shown sub-millitesla magnetic field effects for a flavin-based radical pair. [28, 78] However, the above experiments investigated the effect of the intensity of the field; to function as a compass such reactions must be sensitive to the orientation of the external field. To this end, an artificial system based on a carotenoid-fullerene radical-pair has been shown to exhibit reaction dynamics sensitive to the orientation of an external magnetic field, providing a proof of principle that the radical-pair mechanism can provide directional information, albeit for fields three orders of magnitude larger than the Earth's. [77] Finally, perhaps the most convincing result that the radical-pair mechanism underlies avian magnetoreception is the demonstration of *Earth-strength* magnetic field effects in the aforementioned carotenoid-fullerene system. [55] In particular, it was shown that the response was sensitive to the *inclination* of the external field, consistent with a radical-pair based compass. The reason for the lack of experiments with avian cryptochromes is in part due to the difficulty of isolating them with flavin bound. [95, 63].

Finally, perhaps most convincing so far are the results pertaining to cryptochrome 4, [33, 168, 25, 165] in particular European robin Cry4a, (erCry4a). Numerous lines of evidence suggest erCry4a as the magnetoreceptor: (1) it doesn't display circadian oscillations, thereby ruling out as being involved in circadian rhythms, [25] (2) it is up-regulated in migratory season. [33, 100], and (3) is expressed at a higher concentration in migratory animals than their non-migratory counterparts [33, 165]. Furthermore, erCry4a is located in the outer segments of double cones and long-wavelength single cones, [163] providing the necessary aforementioned orientational ordering.

## 1.2 Discussion

Even with such theoretical and experimental support, conclusive evidence that cryptochrome functions as a magnetoreceptor is still missing. Currently little is known about how it affects cellular activity, and the proteins it interacts with to transduce magnetic information. Tentatively it has been suggested that cryptochrome may interfere with the visual process, producing patterns across the visual field that could be interpreted as north. [66, 110] To this end it has been suggested that cryptochrome may (indirectly) affect glutamate reception; [42] the release rate of glutamate at the cone synapse has been shown to encode light-intensity, thereby providing a direct link between cryptochrome and the visual system. [21] Similarly it has been shown that cryptochrome interacts directly with a potassium voltage-gated channel, thereby providing a link between cryptochrome and the cellular membrane potential – a necessary step in any signal transduction process. Furthermore, there is a discrepancy between the absorption spectrum of flavin and the wavelength cutoff in orientation experiments. Flavin is known to have a fairly sharp cutoff at $\approx 500$ nm in its abosprtion spectrum, however behavioral experiments show that birds can orient up to $\approx 565$ nm. Finally, the effects of light-intensity, in particular the observation of disorientation beyond some threshold ($\approx 10^{12} \frac{\mu\text{mol}}{\text{s m}^2}$ ), have so far been unexplained.

## 1.3 Outline of Thesis

In chapter 2, it is shown in detail how magnetic fields can affect chemical reactions through the radical pair mechanism. In chapter 3 this formalism is applied to model systems to understand how fluctuations in the hyperfine interactions affect the directionally-sensitive reaction yield. In chapter 4 the physical limits of a radical-pair based compass are explored by investigating which nuclear environment (i.e. hyperfine interactions) provide the 'best' re-

sponse, with a comparison to the flavin-tryptophan radical-pair suggested for cryptochrome. In chapter 5 the effects of light-intensity on cryptochrome's photocycle, in particular its signalling state, are explored. Here it is shown that for flavin's photocycle, sufficiently high light-intensities lead to disorientation by deactivating cryptochrome. Finally, in chapter 6 we combine cryptochrome's photocycle with a simple phosphorylation binding model which supports the proposal that the light-indepenent reaction step is magnetically sensitive.

# Chapter 2

# Theory

In this chapter, we illustrate how Earth-strength magnetic fields can affect biochemical reactions involving radical-pair intermediates through the 'radical-pair mechanism', by removing degeneracies in the zero-field Hamiltonian. Such reactions proceed through short-lived, highly reactive, intermediate radical-pairs whose chemical pathway depends on its electronic spin-state, i.e., singlet or triplet, with at least one of these undergoing a reaction not available to the other. The (electronic) spin-state of this radical-pair can be affected by an external magnetic field through the Zeeman interaction, affecting which reaction pathway is taken, thereby providing a physical basis of magnetoreception. In particular, for anisotropic hyperfine interactions, this effect depends on the orientation of the field, thereby providing the basis of a magnetic compass. If the hyperfine interaction is also axial, the response to the magnetic field will depend only on the inclination of the external field (i.e. not the polarity), consistent with the avian magnetic compass.

First we give a brief overview of the spin-formalism and interactions that make up the Hamiltonian. Then using the stochastic Liouville equation we describe how the yield of such a reaction depends on the system parameters, in particular the external magnetic field,

hyperfine interactions, and lifetime of the radical-pair. Finally we illustrate this formalism through model calculations, namely one based on the proposed radical-pair in cryptochrome.

## 2.1 Background

From an energy perspective, it should be impossible for Earth-strength magnetic fields to affect a chemical reaction. [127] However, numerous experimental [50, 23, 77, 55] and theoretical [22, 47] results have shown such an effect is possible. To escape the constraints imposed by energy, it is first necessary to excite the system so that it is in a non-equilibrium state. Indeed, typically radical-pairs are formed upon light-absorption in their singlet (but also triplet [23, 43]) state – neither of which is in equilibrium (i.e. stationary states of the underlying Hamiltonian dynamics). In this non-equilibrium state, small perturbations, e.g., from weak external fields, can alter its dynamics significantly, thereby escaping the energy constraints imposed. [47] Magnetic field effects on reactions were first discovered in nuclear magnetic resonance experiments, [50, 23] and later found to have their origin in reactions involving radical-pair intermediates. [127]

## 2.2 Spin Dynamics

Elementary particles (e.g. electrons, protons, and neutrons), as well as systems formed from them (e.g. atomic nuclei) all contain a purely quantum property known as spin, a form of *intrinsic* angular momentum. Being a form of angular momentum, spin gives rise to a magnetic moment, [48] causing the particle (or system of particles) to interact with magnetic fields. In particular, this magnetic moment can interact with the Earth's magnetic field, and under the right conditions can form the basis of a magnetic compass. Furthermore, this magnetic moment gives rise to its own magnetic field, which other particles with spin will

interact with. This spin-spin interaction, the dipolar interaction, will be shown to be the source of directional information in the avian magnetic compass. The relationship between the (spin) angular momentum and magnetic moment is identical to its classical counterpart:

$$\vec{\mu} = \gamma \vec{S} \tag{2.1}$$

where $\mu$ is the magnetic moment, $\gamma$ is the particle's gyromagnetic ratio (e.g. for electrons $\gamma = \frac{g_e \mu_B}{\hbar}$ where $g_e$ is the electron g-factor and is approximately two, while $\mu_B$ is the Bohr magneton), and $\vec{S}$ is the (spin) angular momentum. For quantum systems, the angular momentum becomes an operator; [114] in particular for spin-$\frac{1}{2}$ particles, these operators are described by:

$$\vec{S} = \frac{\hbar}{2}(\sigma_x \hat{x} + \sigma_y \hat{y} + \sigma_z \hat{z}) \tag{2.2}$$

where $\sigma_x = \left(\begin{smallmatrix} 0 & 1 \\ 1 & 0 \end{smallmatrix}\right)$, $\sigma_y = \left(\begin{smallmatrix} 0 & -i \\ i & 0 \end{smallmatrix}\right)$, and $\sigma_z = \left(\begin{smallmatrix} 1 & 0 \\ 0 & -1 \end{smallmatrix}\right)$ are the Pauli matrices. That is, the spin angular momentum is described by a vector whose components are operators. Electrons, protons, and neutrons are all spin-$\frac{1}{2}$, and in general particles can only have a spin of the form $\frac{N}{2}$ where N is any non-negative integer. A spin-n particle can exist in 2n + 1 states; for the case of spin-$\frac{1}{2}$ this means two states, which are often referred to as 'spin-up' (denoted $|+\rangle$) and 'spin-down' (denoted $|-\rangle$). For a spin-1 system, e.g. the nuclei of 14N (the more abundant isotope of nitrogen), there are three states, typically denoted as $|11\rangle, |10\rangle,$ and $|1-1\rangle$ where the first number describes the spin of the particle, and the second describes the spin measured with respect to the z-axis. The spin operators for a spin-1 particle are: $S_{1x} = \frac{\hbar}{\sqrt{2}}\left(\begin{smallmatrix} 0 & 1 & 0 \\ 1 & 0 & 1 \\ 0 & 1 & 0 \end{smallmatrix}\right)$, $S_{1y} = \frac{\hbar}{\sqrt{2}i}\left(\begin{smallmatrix} 0 & 1 & 0 \\ -1 & 0 & 1 \\ 0 & -1 & 0 \end{smallmatrix}\right)$, and $S_{1z} = \hbar\sqrt{2}\left(\begin{smallmatrix} 1 & 0 & 0 \\ 0 & 0 & 0 \\ 0 & 0 & -1 \end{smallmatrix}\right)$. In general the equations that describe the

spin operators for a spin-n particle are:

$$\langle m'|S_x|m\rangle = (\delta_{m',m+1} + \delta_{m'+1,m})\frac{1}{2}\sqrt{n(n+1) - m'm} \tag{2.3}$$

$$\langle m'|S_y|m\rangle = (\delta_{m',m+1} - \delta_{m'+1,m})\frac{1}{2i}\sqrt{n(n+1) - m'm} \tag{2.4}$$

$$\langle m'|S_z|m\rangle = \delta_{m',m} \tag{2.5}$$

Typically the first step in solving spin Hamiltonians is setting up the spin operators for the system; once this is completed the Hamiltonian can be constructed, and its eigenvalues (i.e. energy levels) and eigenvectors can be constructed, allowing one to calculate the value of any observable of interest (e.g. position, momentum, total spin).

The state of a spin-n system is described by a 2n + 1-dimensional (complex) vector that exists within a Hilbert space, i.e. the wavefunction, denoted $|\Psi\rangle$; typically this abstract quantity is represented concretely as a column vector. To represent the spin state of a particle, it is necessary to have a 'suitable' basis, i.e., a set of vectors that span this Hilbert space. This basis is not unique, and its choice often reflects the symmetry of the underlying problem. To this end, it is necessary to find a complete set of commuting observables to uniquely specify our state. Operators that commute can simultaneously be diagonalized – that is, there exist an eigenbasis common to both. This basis allows us to uniquely describe our state when degeneracies are present – e.g., if there exist two states that have the same energy, then we cannot distinguish them based on their energy alone. What is needed is another observable that commutes with the Hamiltonian such that each of these have a different eigenvalue under this operator, allowing us to describe each state by a pair of eigenvalues.

For quantum systems, physical observables are represented by operators, with their eigenvalues providing the *allowable* values. This implies that their eigenvalues must be real, which can be satisfied by Hermitian operator. Typically this set of eigenvalues is discrete, in contrast to the classical case.

In general, the time-evolution of a spin-system is governed by the Schrödinger equation:

$$i\hbar\frac{\mathrm{d}\left|\Psi\right\rangle}{\mathrm{d}t} = \mathcal{H}\left|\Psi\right\rangle \tag{2.6}$$

where $\mathcal{H}$ is the Hamiltonian describing the system. In cases where the Hamiltonian is time-independent, as considered in this thesis, one can solve this immediately to obtain:

$$\left|\Psi(t)\right\rangle = \exp\left\{-\frac{i\mathcal{H}}{\hbar}t\right\}\left|\psi(0)\right\rangle \tag{2.7}$$

where the (matrix) exponential on the right-hand side is the 'time-evolution operator', i.e., the operator which describes how a state is evolved through time, and $\left|\psi(0)\right\rangle$ is the initial state of the system. In general this matrix exponential is difficult to calculate, but can be simplified by expressing the Hamiltonian with respect to its eigenbasis – in this basis, the Hamiltonian will simplify to a diagonal matrix, thereby allowing one to immediately calculate the matrix exponential (i.e. by taking the exponential of each diagonal element separately). To find this eigenbasis one therefore must solve time-independent Schrödinger equation:

$$\mathcal{H}\left|\Psi\right\rangle = E\left|\Psi\right\rangle \tag{2.8}$$

where E are the eigenvalues (i.e. allowed energies).

### 2.2.1 Zeeman Interaction

For a single spin-$\frac{1}{2}$ particle, an external magnetic field will cause the particle to oscillate between its 'spin-up' and 'spin-down' states. Furthermore, the (average) spin of the particle will precess about the field, in a manner analogouos to a gyroscope. For illustrative purposes we consider the case of an electron, where the Hamiltonian describing the spin-evolution of

this system is again identical to its classical counterpart:

$$\mathcal{H} = -\vec{\mu} \cdot \vec{B} = -\gamma \vec{S} \cdot \vec{B} \tag{2.9}$$

where the coordinate system is typically chosen so that the magnetic field lies along the z-axis (i.e. $\vec{B} = 0, 0, B_z$) so that our Hamiltonian becomes:

$$H = \omega S_z \tag{2.10}$$

where $\omega \equiv \frac{eB}{m_e c}$ where e is the charge of an electron, $m_e$ its mass and c is the speed of light. The average spin in this case is: [114]

$$\langle S_x \rangle (t) = \langle S_x \rangle (0) \cos(\omega t) - \langle S_y \rangle (0) \sin(\omega t) \tag{2.11}$$

$$\langle S_y \rangle (t) = \langle S_y \rangle (0) \cos(\omega t) + \langle S_x \rangle (0) \sin(\omega t) \tag{2.12}$$

$$\langle S_z \rangle (t) = \langle S_z \rangle (0) \tag{2.13}$$

which describes a vector that precesses about the z-axis, i.e., the direction of the magnetic field.

### 2.2.2 Hyperfine Interaction

The origin of the hyperfine interaction is due to the interaction between the magnetic moments of two particles possessing spin. That is, the spin of one of these particles gives rise to a magnetic field, which the other particle interacts with through its magnetic moment (the converse situation is identical). Typically this is considered between the electron and nearby nuclei, i.e., the electron experiences a magnetic field due to nearby nuclei (owing to their spins) and is considered an *internal* field, in contrast to the *external* field in the Zeeman

interaction. The Hamiltonian for the *spin* component of this interaction is:

$$\mathcal{H}_{HFI} = \vec{S} \cdot \vec{\mathbf{A}} \cdot \vec{I} \tag{2.14}$$

$$= \begin{pmatrix} S_{1x} & S_{1x} & S_{1x} \end{pmatrix} \cdot \begin{pmatrix} A_{xx} & A_{xy} & A_{xz} \\ A_{yx} & A_{yy} & A_{yz} \\ A_{zx} & A_{zy} & A_{zz} \end{pmatrix} \cdot \begin{pmatrix} I_{1x} \\ I_{1x} \\ I_{1x} \end{pmatrix} \tag{2.15}$$

where $\vec{\mathbf{A}}$ is the hyperfine tensor, i.e., a $3 \times 3$ matrix representing the interaction, typically expressed in millitesla (mT). We can confirm that this interaction is indeed anisotropic, by showing that it changes under a rotation of our coordinate system. The operator that rotates this Hamiltonian through an angle $\phi$ about, e.g., the z-axis, is given by $\mathcal{D}_z(\phi) = \exp\{-\frac{i}{\hbar} S_z \phi\}$. [114] Furthermore, the Hamiltonian, like any observable, will transform according to $\mathcal{H}' = \exp\{\frac{i}{\hbar} S_z \phi\} \mathcal{H} \exp\{-\frac{i}{\hbar} S_z \phi\}$ which can shown to change the Hamiltonian. We can perhaps see this more clearly by realizing that the Hamiltonian does not commute with $S_z$ so that the rotation will transform the Hamiltonian. In contrast, an isotropic hyperfine interaction, $\mathcal{H} = a\vec{S} \cdot \vec{I}$ will commute with $S_z$ and therefore not depend on the choice of coordinate system. Axial hyperfine interactions are characterized by being unchanged with respect to rotations about the z-axis. In their principal basis (i.e. diagonalized) they take the form $\mathbf{A} = \{a + \alpha, a + \alpha, a - 2\alpha\}$ where 'a' describes the isotropic part, and $\alpha$ the anisotropic part.

### 2.2.3 System of two spin one-half particles

When there are multiple particles possessing spin, one can speak of the *total* spin of the system. In this case we can take as our basis the eigenstates of the *total* spin operator and its *total* projection along the z-axis. For a system consisting of two spin-$\frac{1}{2}$ particles, we can express the state of the system in two different ways: (1) by referring to the spin projected

along the z-axis of each particle (e.g. in this case our states would be described as 'up up', 'up down', etc) or (2) the total spin and its projection along the z-axis, which in this case would be either 'singlet' or 'triplet'. In either case there are four states the system can be in – for case (2) there is one associated with singlet, and three with triplet.

The spin operators for multi-particle systems can be constructed by taking outer products between the constituent operators. For example, in the hyperfine interaction above, the dot product can be expanded to yield an expression containing the following term: $A_{xx}S_{1x} \otimes I_{1x}$ where the symbol $\otimes$ denotes the outer product and is often omitted for clarity. This can be calculated as:

$$A_{xx}S_{1x} \otimes I_{1x} = \frac{\hbar}{2}^2 A_{xx} \begin{pmatrix} 0 & 0 & 0 & 1 \\ 0 & 0 & 1 & 0 \\ 0 & 1 & 0 & 0 \\ 1 & 0 & 0 & 0 \end{pmatrix} \tag{2.16}$$

In addition, the operator $\vec{S^2}$ represents the *total* spin of a system of particles and can be simplified as follows:

$$\vec{S^2} = (\vec{S_1} + \vec{S_2})^2 = \vec{S_1}^2 + \vec{S_2}^2 + 2\vec{S_1} \cdot \vec{S_2} \tag{2.17}$$

where for clarity we have omitted the outer-products. The eigenvectors of this operator operator are:

As we can see, three of these states (i.e. the triplet states) are degenerate (i.e have the same eigenvalue). Therefore, in order to distinguish between them we must introduce an additional operator which commutes with $\vec{S^2}$, i.e. $S_z$. In this way we can uniquely specify each state in terms of its eigenvalues of these two operators.

Any state (i.e. $|\psi\rangle$) of a system composed of two spin-$\frac{1}{2}$ can be expressed in terms of *either* the eigenbasis of $\vec{S^2}$ and $\vec{S_z}$ *or* $\vec{S_{1z}}$ and $\vec{S_{2z}}$. The first pair of operators define the so-called 'singlet-triplet basis', while the second pair defines the 'product-operator basis'. The singlet-

triplet basis is represented by $\{|s=1,m=\pm1,0\rangle, |s=0,m=0\rangle\}$, where the first element in each ket describes the eigenvalue of $\vec{S^2}$ and the second the eigenvalue of $\vec{S_z}$ (N.B. both of these are for the *total* spin operators). Similarly, the product-operator basis is represented as $|{+}{+}\rangle, |{+}{-}\rangle, |{-}{+}\rangle, |{-}{-}\rangle$ where, e.g., the first term in $|{+}{-}\rangle$ denotes that particle 1 is in its 'spin-up' state, while the second particle is in its 'spin-down' state, and similarly for the others. The relationship between these two bases are given by:

$$|s=1,m=1\rangle = |{+}{+}\rangle \tag{2.18}$$

$$|s=1,m=0\rangle = \frac{1}{\sqrt{2}}(|{+}{-}\rangle + |{-}{+}\rangle) \tag{2.19}$$

$$|s=1,m=-1\rangle = |{-}{-}\rangle \tag{2.20}$$

$$|s=0,m=0\rangle = \frac{1}{\sqrt{2}}(|{+}{-}\rangle - |{-}{+}\rangle) \tag{2.21}$$

which can be compactly represented by the following matrix:

$$A = \begin{pmatrix} 1 & 0 & 0 & 0 \\ 0 & \frac{1}{\sqrt{2}} & \frac{1}{\sqrt{2}} & 0 \\ 0 & 0 & 0 & 1 \\ 0 & \frac{1}{\sqrt{2}} & -\frac{1}{\sqrt{2}} & 0 \end{pmatrix} \tag{2.22}$$

i.e., this matrix converts *from* the product-operator basis to the singlet-triplet basis.

### 2.2.4 Density Operator

In the above we have only considered 'pure states', i.e., quantum states which can be described completely by a single wavefunction, $|\psi\rangle$. However, this is not the most general state possible – one can also have 'mixtures' of these pure states. For example, it is often the case that the *initial* state of our system is not known precisely, but instead described statistically through a distribution. In other words, the systems are not prepared identically. We could have an ensemble of such systems, each with an unknown initial state that evolves according to the same Hamiltonian, and ask what the average properties of this ensemble are. In this

situation there are two sources of uncertainty: (1) the uncertainty of our initial state, and (2) the uncertainty imposed on its evolution due to quantum mechanics. The density operator captures both of these effects and is defined as:

$$\hat{\rho} = \sum_{k=1}^{N} p_k \left|\psi_k\right\rangle \left\langle\psi_k\right| \tag{2.23}$$

where $|\psi_k\rangle$ are a collection of pure states (not necessarily orthogonal). Furthermore, 'N' represents the number of states under consideration and can be anything – it is not restricted to the dimension of the Hilbert space. The 'weights', described by $p_k$, represent the distribution describing our state; e.g., this statistical mixture can be taken to be the Boltzmann distribution.

To better illustrate this, suppose we have two spin-$\frac{1}{2}$ systems, one which begins in the state $|+\rangle$ and the other in $(|+\rangle + |-\rangle)/\sqrt{2}$ (i.e. a superposition of 'up' and 'down'). Now we can ask what the average of, e.g., the spin in the z-direction is, $\langle S_z \rangle$. In this case the density operator describing the distribution is:

$$\hat{\rho} = \frac{1}{2}\begin{pmatrix} 1 & 0 \\ 0 & 0 \end{pmatrix} + \frac{1}{2}\begin{pmatrix} \frac{1}{2} & \frac{1}{2} \\ \frac{1}{2} & \frac{1}{2} \end{pmatrix} \tag{2.24}$$

$$= \begin{pmatrix} \frac{3}{4} & \frac{1}{4} \\ \frac{1}{4} & \frac{1}{4} \end{pmatrix} \tag{2.25}$$

Now that we have the density operator that describes the system we can compute $\langle S_z \rangle$; for a pure state, the average of an observable, 'A', is given by $\langle \Psi | A | \Psi \rangle$, however for a mixed state it is $\mathrm{Tr}\{\rho A\}$ so that we have:

$$\langle S_z \rangle = \mathrm{Tr}\{\rho S_z\} = \frac{\hbar}{4} \tag{2.26}$$

Another instance where the density operator formalism is required is for 'open systems. Schrödinger's equation only holds for 'closed' systems, i.e. systems which do not interact with an environment – this is analogous to Newton's laws which only hold in non-inertial reference frames. For open quantum systems, one can extend our system of interest to include the environment, however one cannot typically specify with certainty its state, i.e., it again requires a density operator approach.

## 2.3 Radical Pair Mechanism

A prototypical reaction scheme illustrating the basics of the radical pair mechanism (RPM) is shown in Fig. 2.1. The process begins with light absorption by the donor molecule (D), which triggers an electron-transfer to the acceptor molecule (A), forming a radical pair between molecules D and A. This step is typically spin-conserving, so that the initial (electronic) spin state of the radical pair is the same as its precursor, i.e., singlet. Once the radical-pair is created, it will not remain in its singlet state, as it is generally not an eigenstate of the systems Hamiltonian. Instead it will (coherently) oscillate between its singlet and triplet states, typically due to the hyperfine interaction, although the spin-orbit interaction has also been considered. [64]

This singlet-triplet interconversion can be understood semi-classically – each electron experiences a unique magnetic field owing to their different nuclear environments. Therefore, each electrons *average* spin will precess at a different rate about the resultant field due to nearby nuclei, shown in Fig. 2.3, the effect of which is to cause the electrons to oscillate between their singlet and triplet states. [123, 118, 127] Furthermore, if a weak external magnetic field (i.e. weak compared to the hyperfine coupling strengths) is applied, each electron will now precess about the resultant magnetic field that is a combination of the internal (i.e. nuclear) and external (i.e. Earth's) magnetic fields. In other words, the addition of an external mag-

netic field will affect this interconversion by modifying the hyperfine induced oscillations. Furthermore, if the hyperfine interaction is (axially) anisotropic, [133] then the effect of the external magnetic field will depend on its orientation. In particular, the axial nature of the hyperfine interaction implies that the effect will only depend on the inclination angle, $\theta$, and not the polar angle, $\phi$. In this way, the ST-interconversion depends on the axial nature of the external magnetic field, consistent with the avian magnetic compass.

Finally, competing with this interconversion process are spin-selective reactions unique to each spin-state, described by $k_{\mathrm{S}}$, and $k_{\mathrm{T}}$. That is, the singlet and triplet states react to form unique products, one of which is assumed to initiate an unknown signal transduction pathway. The fraction of radicals (i.e. the yield) decaying through, e.g., the singlet-channel will be proportional to its concentration, which in turn depends on the external magnetic field resulting from ST-interconversion. In this way, the radical-pair mechanism transduces the magnetic field into a biochemical signal whose concentration depends on its inclination, forming the basis of a magnetic compass.

For illustrative purposes it is generally assumed that the decay reactions are spin-independent (i.e. $k_{\mathrm{S}} = k_{\mathrm{T}}$). This uncouples the spin dynamics from the reaction dynamics, enabling a closed form solution. The value for these rate-constants is constrained by the strength of the external magnetic field – if the decay rate is too fast, the external magnetic field will not have sufficient time to induce appreciable ST-interconversion. The Larmor frequency for an Earth strength magnetic field (i.e. i.e. 50 $\mu$ T) is on the order of 10 $\mu$ s, suggesting that the radical-pair must have a lifetime on this timescale for the external field to have an effect.

Without loss of generality we assume that the triplet state reaction pathway leads to a biologically active product. We are interested in the fraction of radicals that decay through this triplet channel, particularly how it depends on the fields orientation. Assuming a first

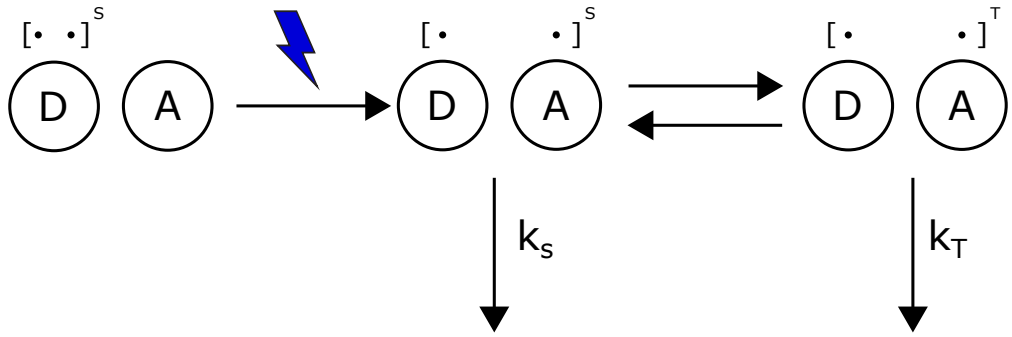


Figure 2.1: Before light absorption, molecule D contains two electrons in a closed shell, and are therefore in the singlet state. Upon light absorption, an electron transfers to molecule A, forming a radical pair between them; this process is spin-conserving so that the initial state of the radical-pair is also a singlet. The radical-pair will then undergo two competing processes: (1) Hamiltonian driven singlet-triplet interconversion and (2) spin-selective decay from each of the spin-states. If the interconversion step depends on the orientation of, e.g., the Earth's magnetic field, then so too will the products, thereby encoding directional information into the chemical yield of the system.

order decay process, the yield of radicals decaying through this channel is given by:

$$\Phi^{\mathrm{T}} = \int_0^\infty k_{\mathrm{T}} T(t)\,\mathrm{d}t \tag{2.27}$$

where T(t) is the fraction of radicals in the triplet state at a given time. This can be obtained from the spin-dynamics of the system. In particular, the average number of radicals in the triplet state is given by:

$$T(t) = \mathrm{Tr}\Big\{Q^{\mathrm{T}}\rho(t)\Big\} \tag{2.28}$$

where $Q^{\mathrm{T}}$ is the triplet-projection operator, i.e., the operator such that $Q^{\mathrm{T}}\left|T\right\rangle = 1$, while being zero for a non-triplet (i.e. singlet) state. In general the trace of an operator A, $\mathrm{Tr}\{A\rho\} = \sum_i (A\rho)_{ii}$, is the average value for that operator; when the operator is a projection operator, this gives the average number of systems in that state.

To continue we need to explicitly solve for the density-operators spin-dynamics. Its evolution will be due to the two aforementioned competing processes: (1) singlet-triplet interconver-

sion, described by the systems Hamiltonian and (2) spin-selective recombination. The first process can be described through the Schrödinger equation, while the second must be described phenomenologically, i.e., not from first principles. [34] The reason for this is that the Schrödinger equation cannot describe decay unless the Hamiltonian is imaginary. Therefore the standard quantum-mechanical equations of motion are extended to capture this effect via the stochastic Liouville equation: [61]

$$\frac{\mathrm{d}\rho}{\mathrm{d}t} = -\frac{i}{\hbar}[\mathcal{H},\rho] - \frac{k_{\mathrm{S}}}{2}\Big\{Q^{\mathrm{S}},\rho(t)\Big\} - \frac{k_{\mathrm{T}}}{2}\Big\{Q^{\mathrm{T}},\rho(t)\Big\} \tag{2.29}$$

Where square brackets denote the commutator of the two operators, i.e. $[A,B] = AB - BA$ while the curly brackets denote the anti-commutator, i.e., $\{A,B\} = AB + BA$. Considering, e.g., *only* the second term above describing singlet-decay, it can be shown that the singlet population is decays according to a first-order process, i.e., $\langle S\rangle = \mathrm{Tr}\big\{S\rho(t)\big\} = \frac{1}{2}(1 + \exp(-k_{\mathrm{S}}t)$. [34]

In the case where $k_{\mathrm{S}} = k_{\mathrm{T}}$, a formal solution can be obtained for *time-independent* Hamiltonians:

$$\rho(t) = \exp\left(-i\frac{\mathcal{H}t}{\hbar}\right)\rho(0)\exp\left(i\frac{\mathcal{H}t}{\hbar}\right) \tag{2.30}$$

where $\rho(0)$ is the initial state of the system, i.e. the spin-state of the nuclei and electrons. As mentioned previously, the initial spin-state of the electrons is a singlet, while the nuclei are assumed to be in thermal equilibrium. In other words, the density operator describing the initial electronic spin-state is $\rho(0)_{\mathrm{electronic}} = Q^{\mathrm{S}}$ while the nuclear spin-state is $\rho(0)_{\mathrm{nuclear}} = \frac{\mathbb{1}}{N}$ where N is the number of nuclear states, and taking their outer product to from the total density operator gives: $\rho(0) = \frac{Q^{\mathrm{S}}}{N}$

Plugging (2.30) into (2.28) with the appropriate initial condition yields:

$$T(t) = \frac{1}{N}\exp\{-kt\}\sum_{m=1}^{4N}\sum_{n=1}^{4N} Q^{\mathrm{S}}_{mn}Q^{\mathrm{T}}_{mn}\cos\big((\omega_m-\omega_n)t\big) \tag{2.31}$$

where the factor of four in the summation results from the four electronic spin-states (e.g, three triplet plus one singlet) and $\hbar\omega_m$ represents energy corresponding to the Hamiltonian eigenstate $|m\rangle$. Finally, integrating this over all times produces the desired yield:

$$\Phi^{\mathrm{T}} = \frac{1}{N}\sum_{m=1}^{4N}\sum_{n=1}^{4N} Q^{\mathrm{S}}_{mn}Q^{\mathrm{T}}_{mn}\frac{k^2}{k^2+(\omega_m-\omega_n)^2} \tag{2.32}$$

Care must be taken to ensure that the projection operators are expressed with respect to the eigenbasis of the Hamiltonian for this solution to be valid.

Looking at (2.31) better illustrates the effect of the weak external magnetic field. In the absence of an external field, and assuming there exists degeneracies in the zero-field Hamiltonian, these degenerate states will not oscillate (i.e. the cosine term becomes unity). The effect of a weak external magnetic field acts by lifting these degeneracies, [16, 132] thereby increasing ST-interconversion. For a singlet-born radical pair, this increase in ST-interconversion means there will be an increase in the fraction of radicals in the triplet state, and therefore in the triplet yield.

The results above hold for any time-independent Hamiltonian; to better illustrate the results we consider a simple radical-pair based on a flavin-tryptophan radical pair that has been suggested to occur in the putative magnetoreceptor cryptochrome. [110, 22, 41] This system contains a single nuclei on each radical – on the flavin radical the nuclei is taken to be a nitrogen-atom, which has been shown to provide the dominant contribution [22, 41]. For the tryptophan radical the nuclei is taken as a hydrogen atom for the same reason. The Hamiltonian for this system (and indeed any radical-pair with a single nuclei on each radical)

is given by:

$$H = g\mu_{\mathrm{B}}(\vec{S}_1 + \vec{S}_2) \cdot \vec{B} + \vec{S}_1 \cdot \vec{A}_1 \cdot \vec{I}_1 + \vec{S}_2 \cdot \vec{A}_2 \cdot \vec{I}_2 \tag{2.33}$$

where the first term describes the Zeeman interaction with each electron; g is the so-called 'electron g-factor', i.e. g = 2, and $\mu_{\mathrm{B}}$ is the Bohr magneton. The magnetic field can be expressed as:

$$\vec{B} = |B|(\sin(\theta)\hat{x} + \cos(\theta)\hat{z}) \tag{2.34}$$

where $|B|$ is its magnitude and we have let $\phi = 0$ owing to the axial nature of the (anisotropic) hyperfine interaction. Continuing, the second term describes the (anisotropic) hyperfine interaction between the electron and nuclei on radical one and similarly for the third term. In these last two terms, $\vec{S}_i$ is the spin-operator for the electron on radical i. Similarly, $\vec{I}_2$ for the hydrogen nuclei is the same as it is also spin-$\frac{1}{2}$, i.e., $\vec{I}_2 = \vec{S}_1 = \vec{S}_2$. However, the spin-operator for the spin-1 nitrogen is different, given by $S_{1x} = \frac{\hbar}{\sqrt{2}}\begin{pmatrix} 0 & 1 & 0 \\ 1 & 0 & 1 \\ 0 & 1 & 0 \end{pmatrix}$, $S_{1y} = \frac{\hbar}{\sqrt{2}i}\begin{pmatrix} 0 & 1 & 0 \\ -1 & 0 & 1 \\ 0 & -1 & 0 \end{pmatrix}$, and $S_{1z} = \hbar\sqrt{2}\begin{pmatrix} 1 & 0 & 0 \\ 0 & 0 & 0 \\ 0 & 0 & -1 \end{pmatrix}$. Finally, $A_i$ is a $3 \times 3$ matrix that describes the anisotropic hyperfine interaction. The hydrogen anisotropic hyperfine tensor is given by diag(0, 0, 1.0812)mT while the nitrogen tensor is given by diag(-0.2, -0.2, 1.7569)mT. Finally, the lifetime of the radical pair is taken to be $10\mu$s. [41] Using Eq. 2.32, we can calculate the yield for this system, with the result shown in Fig. 2.2

Note that we have ignored various terms in this simple model, including the nuclear Zeeman interaction terms, and inter-radical interactions. In general these terms will remove degeneracies in the zero-field Hamiltonian, which is precisely the mechanism by which the external magnetic field effects occur. In other words, for strong inter-radical interactions (e.g. exchange and dipolar), a weak magnetic field will not have an effect. Since the magnetic moment of the electron is about three-orders of magnitude larger than nuclear

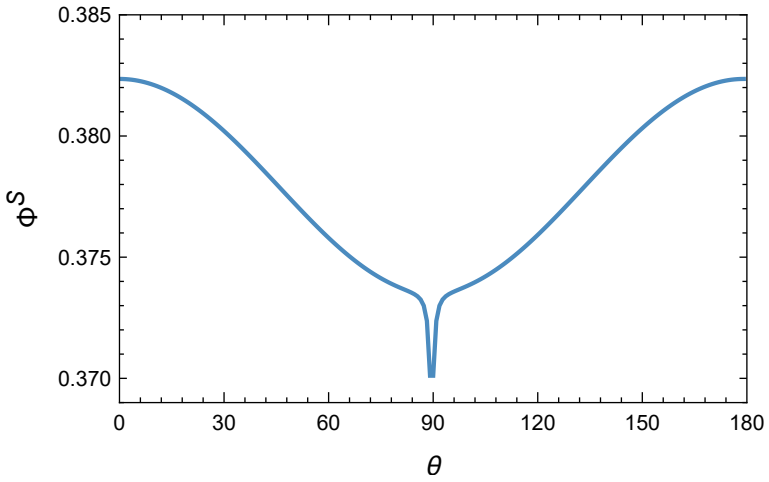


Figure 2.2: Singlet yield for a flavin-tryptophan based radical pair demonstrating a high degree of angular sensitivity. The parameters characterizing this yield are given as follows – the flavin hyperfine interaction is diag(-0.2, -0.2, 1.7569)mT while the tryptophan hyperfine interaction is given by diag(0, 0, 1.0812)mT. The liftime of the radical pair is taken to be $10\mu$s.

magnetic moments, this first approximation is well-justified. Similarly, for radicals that are sufficiently-separated in space we can likewise neglect the inter-radical interactions. For example, the dipolar coupling between the electron of one radical with nuclei of the other radical varies as $\frac{1}{r^3}$. [14] Theoretical calculations suggest that a separation of $>$ 3.5 nm is sufficient to ignore these interactions, and furthermore that at the particular distance of $2 \pm 0.2nm$ [24] these terms may 'cancel' out. Sufficiently large radical-pair separations [52] have been suggested in the literature owing to a chain of conserved tryptophan amino-acids which sequentially transfer the electron towards the flavin, thereby increasing the distance, shown in Fig. 2.3. Furthermore, there is evidence that a fourth tryptophan residue is involved, [87, 94, 51, 168, 160, 165] thereby further increasing the radical-separation distance, allowing a weak magnetic field to overcome their deleterious effects.

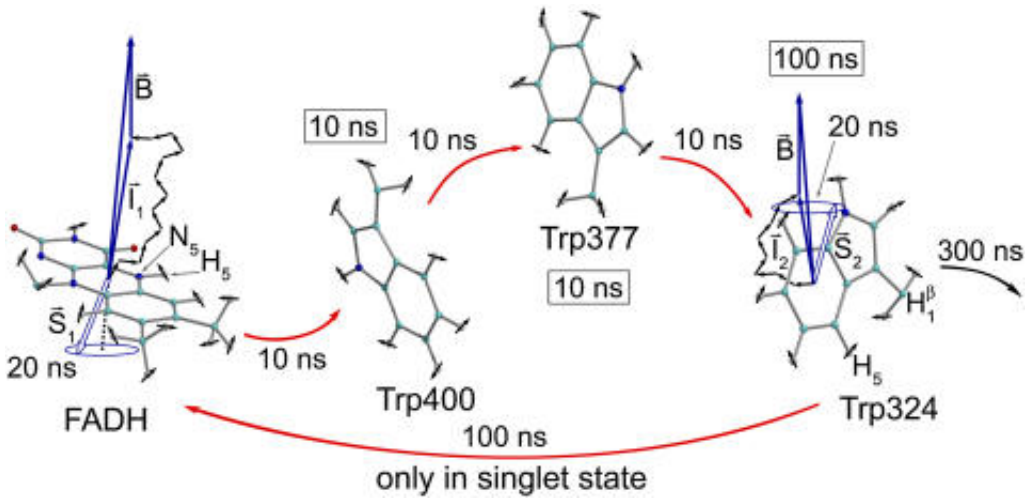


Figure 2.3: Flavin-tryptophan radical pair scheme. [123] Light absorption by flavin (FADH) causes an electron-hole to transfer, along a chain of nearby tryptophan residues, resulting in a radical-pair between FADH and Trp324. Recombination back to the ground state occurs only from the singlet state.

## 2.4 Discussion

In the above we have presented a simple model that illustrates how a *weak* external magnetic field can affect the spin-dynamics of a radical pair, thereby altering which reaction pathway is taken. A number of simplifications have been made, most severely the neglect of spin decoherence and relaxation. Their inclusion is outside the scope of this thesis, but are briefly described for completeness sake. In general, spin-relaxation is due to the discarded terms from the Hamiltonian whose exact description is ignored and is instead described phenomenologically. The main source of relaxation in the system under study is due to time-dependent modulations of the hyperfine interaction, particularly as the molecules rotate and move in space. [29]

# Chapter 3

# Yield for Fluctuating Hyperfine Interaction

Recently it has been shown that the avian magnetic compass due to the radical pair mechanism is more sensitive than previously thought possible. Avoided crossings in the energy spectrum can produce a singlet yield with a singular spike, described as a "quantum needle". [41] Since the compass sensitivity likely relies on the variation of the yield, this represents a significant improvement in its performance; [97] all systems considered prior were found to have a smoothly varying signal. While it is important that the compass be sensitive, it must also be robust to variations of parameters in the model. Typically, these variations are due to fluctuations in distance of the two radicals and orientation of the molecule, due to the thermal bath, modulating any distance dependent parameters such as the hyperfine interaction and decay rate. A relatively minor decrease in the decay rate, or change in the hyperfine structure, can be enough to significantly affect the yield, and perhaps destroy the needle. [106] In this chapter we show that fluctuations in the hyperfine interactions unexpectedly *improve* the needle by increasing its depth. Furthermore, it is found that such fluctuations provide robustness against variations in the decay rate, with minimal loss in sensitivity

## 3.1 Background

Birds are known to migrate thousands of kilometers to the same location each year to breed and search for food. [6, 82] This suggests the use of a highly precise map and compass. In particular, the magnetic compass has been suggested [41] to have the necessary precision. It has been found that the flavin-tryptophan radical-pair formed in cryptochrome produces a signal with a needle-like feature, giving rise to a high degree of directional sensitivity. [41] The origin of this needle is due to an avoided crossing in the energy spectrum with respect to the inclination angle. Any avoided crossing is characterized by two features: (1) it's separation of closest approach, and (2) the angle at which these levels approach one another. The latter can also be understood in terms of the separation of *furthest* approach, i.e., the separation far away from the avoided crossing. [102]

We can understand the role of the avoided crossing as follows: as one moves away from the angle of closest approach, the energy separation is large, little singlet-triplet interconversion occurs, and consequently there is little change in the yield. Near the avoided crossing the energy separation is smaller, leading to a significant change in the yield. In other words, only a significant amount of change occurs at inclination angles near the avoided crossing, i.e., a yield with a singular spike. Since sensory systems often detect *changes* in their environment rather than absolute values, [122] this indeed represents a significant improvement.

Because the electrons that constitute the radical-pair are delocalized in space, they will interact with numerous nearby nuclei. For the flavin-tryptophan radical-pair considered [41] this includes up to 21 nuclei – however, it was found that only a few of these nuclei interactions dominate. [41, 22] Therefore, one can consider instead a simplified model with only the largest hyperfine interactions. In particular, for flavin there is a single nitrogen nuclei, while for tryptophan a single hydrogen nuclei. In the following, we base our calculations on this simplified system. Interestingly, this simple system was shown to produce a less promi-

nent needle, [41] suggesting that, at least in some cases, introducing more nuclei increases sensitivity. Finally, it was found that as the lifetime of the radical pair is decreased, the size of the needle deteriorates rapidly, requiring at least $\approx 10\mu$s in all cases considered to see an appreciable signal. In the actual flavin-tryptophan radical-pair, lifetimes on the order of milliseconds are required to observe a needle – far too long to be realized in a biological system. Indeed, these long lifetimes are likely why it went unnoticed despite being considered before. [22]

Although the 'quantum-needle' discovered displays a large directional sensitivity, it must also be robust to variations of parameters in the model. Numerous sources of noise are present, including fluctuations due to being in contact with a thermal bath, as well as inhomogeneity among the cryptochrome molecules themselves. [106, 107] Cryptochrome exists in distinct conformational states, e.g., in dimerized form, with ATP bound, and phosphorylated, with each expected to have a unique local environment. Recently it has been shown [106] that for some radical-pair systems, minor perturbations in the hyperfine interactions can lead to significantly different signals. Therefore, in the following we investigate the effect of fluctuating hyperfine parameters on the quantum needle.

In this chapter we model thermal noise by allowing the hyperfine parameters to fluctuate according to a Gaussian distribution. The strength of this noise is taken as the variance of the distribution – i.e., larger variances correspond to more noise. It is found that by allowing the hyperfine parameters to vary up to 10% improves the depth of the needle, but beyond this leads to degradation. Furthermore, such fluctuations also enable the needle to be present for lifetimes an order of magnitude smaller than those originally considered. These improvements are due to the fact that the flavin-tryptophan parameters are not 'optimal' – the noise therefore causes the system to explore more optimal sets of parameters, which overwhelmingly dominate the average characteristics of the yield. The origin of these effects are due to the small perturbations significantly affecting the avoided crossing distance.

Finally, we consider the case of starting from a more optimal set of hyperfine parameters. Indeed, it could be the case that the effect of the noise is to simply explore the parameter space more fully and favor the optimal ones. However, it is found that starting from a better set of parameters, introducing noise still improves the system. In particular, it is found that here the effect of noise modestly reduces the sensitivity, however, it still provides robustness to variations in the decay rate, allowing it to operate for lifetimes that are an order of magnitude smaller than those previously considered. These calculations suggest that different sets of parameters favor a 'sensitive' needle versus a 'robust' one. Indeed, there appears to be an inherent trade-off between sensitivity and robustness.

## 3.2 Fluctuating Hyperfine Interaction

In the following, we model noise by allowing the hyperfine parameters to fluctuate according to a Gaussian distribution. The (static) flavin hyperfine tensor is described by the diagonal matrix $\mathbf{A_1} = \{-0.2, -0.2, 1.7569\}$ mT, while the tryptophan is $\mathbf{A_2} = \{0, 0, 1.0812\}$ mT. [41, 22] Each component is now instead described through a Gaussian whose average is equal to the static values, with larger widths (i.e. variance) of this distribution simulating the amount of noise. To illustrate this, in Fig. 3.1(A) the distribution for $A_{1xx}$ is shown, with the standard deviation chosen to be $7.8\mu$T. This corresponds to approximately a maximal 10% change in the strength of the interaction. The smallest variance considered is $1.3\mu$T and corresponds to approximately a 1% change in the parameters. Each distribution is drawn independently, and with the same variance. In each case, 1000 samples are drawn, the singlet-yield is calculated for each, and finally these yields are then averaged to obtain the (average) singlet yield.

The results of this process for varying standard deviations are shown in Fig. 3.1(B), where it is found that increasing the amount of noise significantly improves the depth of the needle.

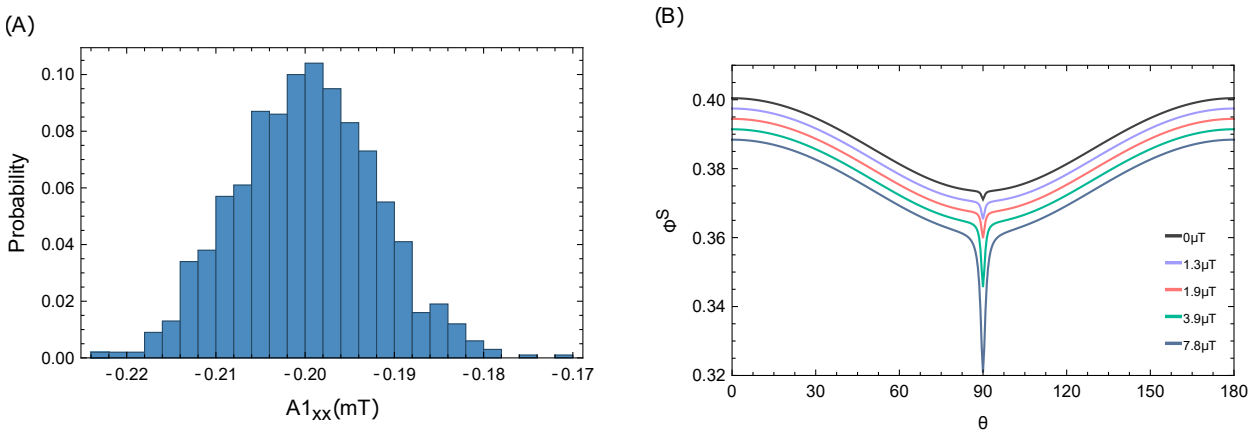


Figure 3.1: (A) For illustrative purposes, we show the hyperfine distribution of the x-component for a variance of $7.8\times10^{-3}$ mT. (B) The yield for different hyperfine distributions; the variance of the fluctuations are taken to be $(1.3, 1.9, 3.9, 7.8)\mu$T. To better see the plots, they are shifted vertically by (0, -0.003, -0.006, -0.009, -0.012). Here we see clearly that increasing noise improves the 'sensitivity' of the needle.

Beyond this, further increases lead to degradation. The source of this improvement lies, in part, due to the fact that the noise is selecting more optimal hyperfine parameters. While it is also the case that noise will select worse parameters, the effect is apparently dominated by the better ones. In other words, the actual parameters describing the flavin-tryptophan are not optimal, and by introducing noise, the system now explores these parameters whose contributions dominate the averaging process. In addition to providing a larger needle, these fluctuations also improve robustness to variations in the decay rate. That is, the needle persists for lower lifetimes under fluctuations, as seen in Fig. 3.2. For the original parameters, the needle disappears completely for a radical-pair lifetime of $2\mu$s, however with noise the needle persists even down to this short lifetime, with minimal loss in sensitivity.

It was expected that in the best case, the effect of this noise would slightly degrade the needle, however, we have found that there is an improvement, namely through its depth. Interestingly, these results do not hold if we impose the constraint $A_{1xx} = A_{1yy}$, suggesting that, at least partially, the results can be understood in terms of breaking this symmetry.

Both of these results can be understood as follows – the effect of the fluctuating hyperfine

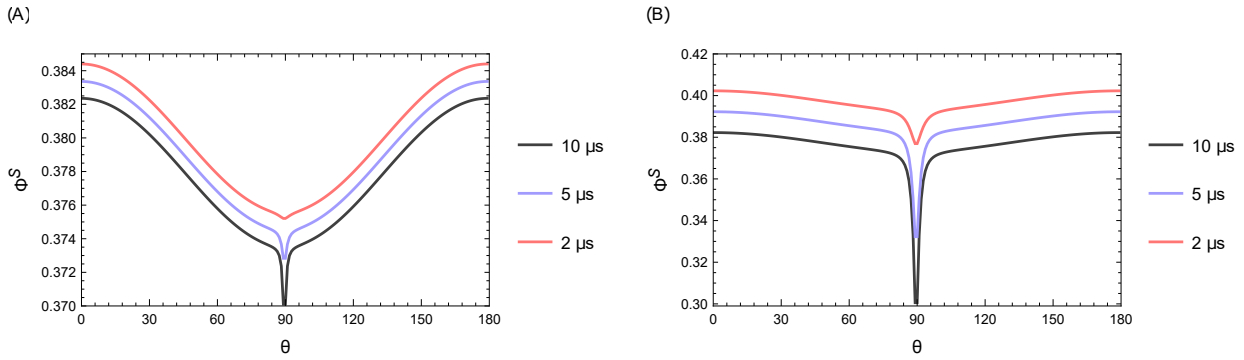


Figure 3.2: (a) The original hyperfine parameters lead to a yield that rapidly deteriorates as the lifetime is decreased. (b) Considering a single fluctuation (i.e. $A_1$ = (-0.21, -0.205, 1.7569)) mT shows a yield that persists even for lower lifetimes.

interaction is to decrease the avoided crossing separation, shown in Fig. 3.3(B). In turn, this lower energy-separation increases the singlet-triplet interconversion (2.31) frequency which has two effects: (1) the triplet yield is increased (i.e. singlet yield is decreased) at the avoided crossing (i.e. $\theta = 90°$), while simultaneously being decreased for angles away from it, and (2) the amount of time needed for the external magnetic field to act is reduced as the frequencies of oscillations are now increased, owing to a smaller energy separation. The approximation of averaging the fluctuations to obtain the singlet yield is valid as long as the fluctuations occur on a timescale much lower than the lifetime of the RP – in the next section the other cases will be considered (i.e. fluctuations on the timescale of the RP lifetime, and much larger).

Finally, we consider the case where we begin from a perturbed set of hyperfine parameters that are more sensitive than the original, and consider the effect of allowing them to fluctuate. In this case, the variance of the hyperfine parameter distributions is taken as $1\mu$T. In this case (see Fig. 3.4) it is found that fluctuations broaden the yield (i.e. in the top plot), thereby reducing the sensitivity. However, it is found that the robustness still persists, providing a needle down to radical-pair lifetimes of $2\mu$s. The origin of this effect can again be understood in terms of the avoided crossings – in this case, the avoided crossing distance will *increase* in response to noise, causing the singlet-yield to broaden. However, the angle at which

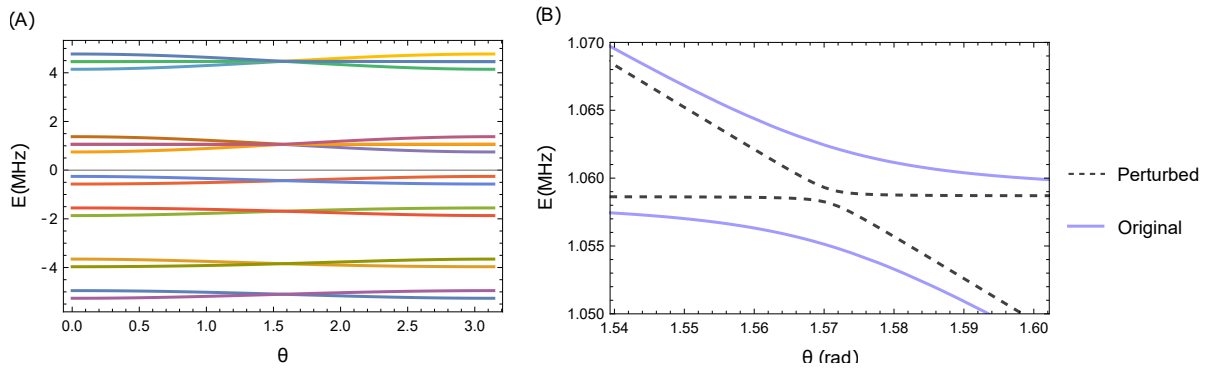


Figure 3.3: (A) The energy spectrum for the simplified flavin-tryptophan radical-pair, displaying a number of 'bands'. (B) Zooming in on these bands displays two avoided crossings (only one is shown for clarity). Furthermore, the distance at their closest approach is reduced upon introducing noise to the system.

the avoided crossings approach (i.e. the distance between the energy levels far from the avoided crossing) are correspondingly decreased. This overall decrease, as mentioned before, will cause the singlet-triplet interconversion frequency to increase for *all* angles, thereby providing a needle for lower lifetimes.

## 3.3 Oscillating Hyperfine Interaction

So far we have assumed that the fluctuations occur much slower than the decay rate, allowing us to simply average our yield over an ensemble of HF parameters. Instead, now we will consider the case where the fluctuations vary sinusoidally and consider three limiting cases – fluctuations that are: (1) much slower, (2) on the same timescale, and (3) much larger, than the lifetime of the radical pair. In this case, it is assumed that each HF parameter varies sinusoidally, each taking the form: $A_{i_{jj}}(0) + C_{i_{jj}} \sin 2\pi f_{i_{jj}} t$ where $i \in (1,2)$, $j \in (x,y)$ and $C_{i_{jj}}$ is the amplitude of the fluctuation. We compare these calculations with the static case. The lifetime of the radical pair is chosen to be 10 $\mu$s in each plot of Fig. 3.5. In the top plot we have chosen $C_{1_{xx}} = \frac{1}{500}$mT, $f_{1_{xx}} = \frac{1}{50}$MHz, $C_{1_{yy}} = \frac{1}{400}$mT, $f_{1_{yy}} = \frac{1}{60}$MHz. This corresponds to the case where the fluctuations are slower than the lifetime, and is analogous

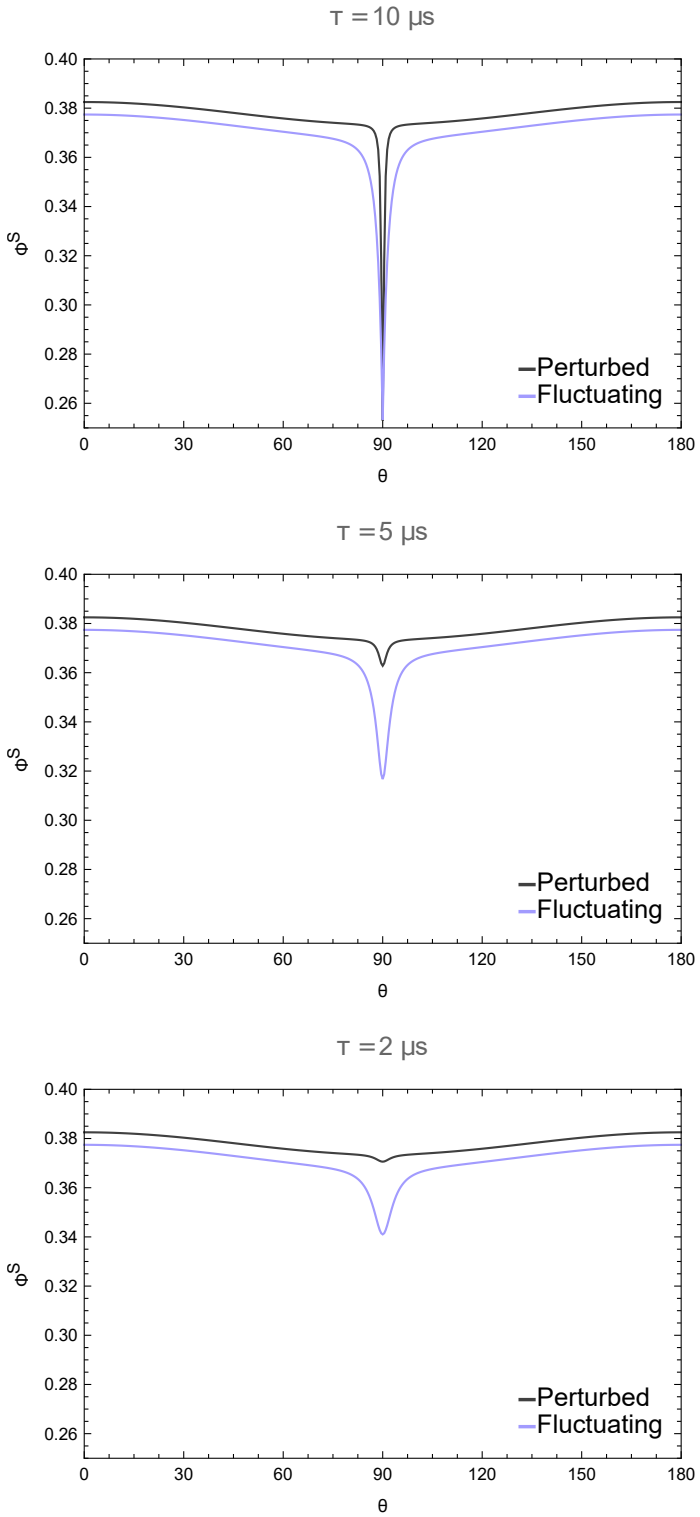


Figure 3.4: Starting from a improved set of hyperfine parameters (e.g. $\mathbf{A}_1 = \text{diag}(-1.982, -1.978, 1.7569)\text{mT}$), hyperfine fluctuations are shown to improve robustness to variations in decay rate. In the top plot the lifetime is $10\mu$s, the middle $5\mu$s while the bottom is $2\mu$s. The standard deviation of the Gaussian distribution describing the fluctuations is $1\mu$T

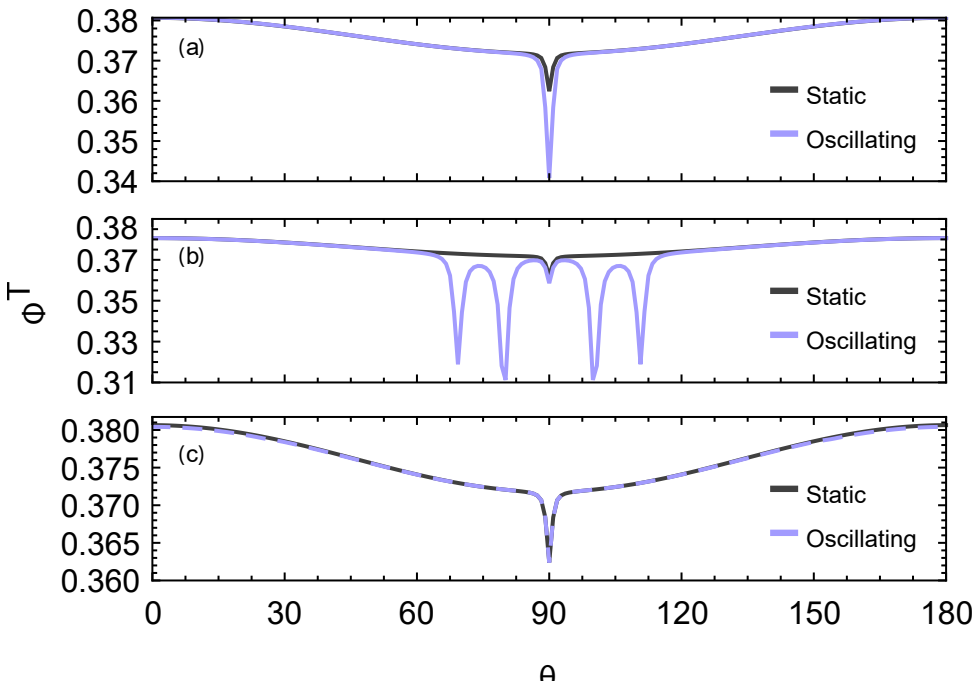


Figure 3.5

to the case where we allowed the parameters to fluctuate according to a Gaussian distribution. The sinusoidal time-dependence is chosen to approximate the Gaussian fluctuations above, supporting our earlier approximation of drawing each HF parameter from a Gaussian and averaging. In the middle plot, everything remains the same, except now $f_{1_{xx}} = \frac{1}{2}$MHz, $f_{1_{yy}} = \frac{1}{4}$MHz; interestingly if $f_{1_{xx}} = f_{1_{yy}}$ there is no change. In this case, we see that the yield is complex, and represents an intermediate state that appears unpredictable and undesirable. Other spikes are now present, likely disrupting the compass. Lastly, in the bottom plot we let $f_{1_{xx}} = 5$MHz, $f_{1_{yy}} = 6$MHz so that the fluctuations occur faster than the radical-pair lifetime. In this case, we see that the fluctuations average out and match the static case. In the above analysis, we see that three regimes emerge: fluctuations occurring on a time-scale smaller, larger, and comparable to the lifetime of the radical pair. We can see that for the fluctuations in the hyperfine interaction to provide robustness, they must be smaller than the lifetime, with similar conclusions being made elsewhere. [52]

## 3.4 Discussion

In this chapter, we have shown that hyperfine fluctuations can both: (1) improve the depth of the quantum needle and (2) improve the lifetime for which the needle persists by about an order of magnitude. Furthermore, we have shown the source of this improvement is due to a decrease in the avoided crossing in the energy spectrum. Finally, one could instead consider the case of starting from a more optimal set of parameters than the one used. In this case, there will still be improvements, however not as dramatic. In particular, there is an inherent trade-off between the sensitivity (i.e. width of the needle) and its robustness. Starting from a more optimal set of parameters reduces the sensitivity, while still improving the robustness. Although counter-intuitive, this has been explored in similar systems, [52, 18, 101]

# Chapter 4

# Optimal Nuclear Environment

In this chapter we use the 'optimality' metric to calculate the optimal hyperfine tensor for various radical-pair systems. Specifically, we consider a radical-pair with one radical devoid of hyperfine interactions, while the other contains one spin-$\frac{1}{2}$ nuclei where it is found that such a system can produce a needle-like feature that persists for radical-pair lifetimes down to $2\mu$s. Next, we consider a flavin based radical pair and calculate the optimal partner for the two cases of spin-$\frac{1}{2}$ and spin-1 nuclei. Here it is found that for a spin-$\frac{1}{2}$ radical-pair the partner radical is similar to the suggested tryptophan radical. This suggests that: (1) the optimal partner to flavin is indeed tryptophan and (2) that it operates near its limits for this simplified system. In this chapter we use the following abbreviation: NMRP refers to a radical pair with N nuclei on one radical, and M on the other. For example, a 10RP would be a radical pair in which one radical contains a single nuclei, while the other contains none.

## 4.1 Backgroud

Any biochemical mechanism that is magnetically sensitive is notable, as it is difficult to explain how weak (i.e. less than 1T), can alter its rate or yield. [127] The radical pair mechanism in particular faces numerous difficulties: spin-relaxation [29, 162], inter-radical interactions [9], rotational disorder, [38, 65] and low-light conditions [82, 39] all pose considerable difficulties to its functioning. In the case of inter-radical reactions, e.g., degeneracies in the zero-field Hamiltonian are lifted, thereby reducing the effects of a weak external field which acts by removing them. [132] These considerations seem to suggest that any magnetoreceptor is therefore optimized, i.e., is both sensitive to changes in the magnetic field, and robust to variations in system parameters, [106, 107, 11] e.g., inter-radical separation, which induces spin-relaxation. [29]

Indeed, numerous approaches have been taken to understand the optimal system parameters for a radical-pair based magnetoreceptor. [113, 107, 17, 111, 43, 109, 68, 7, 51] For example, multiple approaches have considered the case where a radical is devoid of hyperfine interactions, which provides a more sensitive compass. [17, 113, 111] Similarly it has been shown that effects of rotational disorder can be overcome by model systems. [65, 38] In a different direction, attempts have been made at increasing the sensitivity by introducing additional components to the system, e.g., radical scavengers [51], a non-singlet initial radical-pair, [43] and modifications to the cryptochrome reaction dynamics. [97]

Recently, a system based on a flavin-tryptophan radical-pair [22] was found to exhibit a high degree of directional sensitivity, referred to as a 'quantum-needle'. [41] It was suggested that this could be the origin of the highly precise navigational abilities of migrating birds. [82] Its origin was shown to be due to an avoided crossing in the energy spectrum and can be understood as follows: at the avoided crossing, the energy separation is smallest, and therefore singlet-triplet interconversion is largest. Moving away from this value the energy

separation increases rapidly, so that the ST interconversion decreases. In effect, the avoided crossing leads to a significant amount of ST-interconversion, and therefore magnetic sensitivity, only near the avoided crossing. However, the effect requires a lifetime on the order 1000 $\mu$s (and $\approx$10 $\mu$s for a correspondingly simplified system) which would be difficult to meet in any system, especially a biological one characterized by significant noise. Therefore, it is desirable to understand if this needle-like feature can persist for shorter lifetimes. Furthermore, it is not clear whether other systems display this feature or if it is unique to a flavin-based radical-pair; of particular interest are radical-pairs with one radical devoid of significant hyperfine interactions, which typically display high sensitivity. [17, 113] Experiments with oscillating magnetic fields have demonstrated that disorientation occurs when their frequency is at the Larmor resonance, suggesting that one of the radicals is devoid of hyperfine interactions. [44, 130, 134, 53]

Therefore, we search the hyperfine parameter space to see whether other systems can produce such features. However, a brute-force search is too computationally expensive, and does not lend itself to more complicated systems with multiple nuclei, spin-relaxation, and other effects. The presence of a needle is difficult to quantify, and furthermore, may be too restrictive. For example, such a constraint would exclude systems that contain a 'needle-like' feature which could persist for short-lifetimes. Therefore, we use a proxy to describe the performance of the system. Various metrics have been put forth including 'anisotropy', [17] which measures the difference between the maximum and minimum signal values; 'directionality', [97] which measures the spread in the angular-distribution; and 'optimality' [97] which combines the previous two. However, 'anisotropy' does not take into account the

spread in the yield; therefore we use optimality.

$$R_{\text{relative}}(\theta) = \frac{R_{\max} - R(\theta)}{R_{\max}} \tag{4.1}$$

$$\text{Efficiency} = \max\left\{R_{\text{relative}}(\theta)\right\} \tag{4.2}$$

$$\text{Directionality} = \frac{\langle R(\theta)\rangle_\theta - R_{\min}}{R_{\max} - R_{\min}} \tag{4.3}$$

$$\text{Optimality} = \text{Efficiency} \times \left|100\% - 2 \times \text{Directionality}\right| \tag{4.4}$$

Using optimality as the function that we want to maximize, we can now use numerical algorithms to search this space. To this end we have chosen the Nelder-Mead and differential evolution [129] algorithms, in part because they do not require an analytical expression of the derivative, are valid for nonlinear optimization (i.e. the case here), and can incorporate constraints. Furthermore, differential evolution seeks to find the *global* optimum. With this method we can now investigate various model systems. In the following we consider two in particular: (1) a radical pair with one radical containing a single spin-$\frac{1}{2}$ nuclei while the other is devoid (i.e. a 10RP) and (2) a radical-pair with one radical being based on flavin and the other containing one nuclei (i.e. a 11RP); both the spin-$\frac{1}{2}$ and spin-1 cases are considered. In the first case, we are interested in whether the simplest radical-pair system can display a needle. For the second case our motivation was two-fold: (1) the partner radical to flavin has been debated in the literature [44, 113, 124] and (2) such a solution provides a benchmark with which to compare a flavin-tryptophan based radical-pair.

## 4.2 Optimization Using Nelder-Mead and Differential Evolution

The problem of finding a global optimum in a multi-dimensional space is computationally difficult, so we restrict ourselves to simple systems, ignoring inter-radical interactions, spin-relaxation, etc., as done elsewhere in the literature. Therefore, our model Hamiltonians consist of the Zeeman and hyperfine interactions. In the system of study there are numerous parameters that can be adjusted, e.g., the number of nuclei bound to each radical, their spins, the lifetime of the radical pair, and the hyperfine interactions. Since we are interested in finding systems with a 'needle-like' feature for *short* lifetimes, we restrict our search by setting the lifetime to be $2\mu$s. In addition, we constrain the hyperfine parameters to be biologically feasible, i.e. $\leq |0.5|$ mT.

Although each method is different, they both work in a similar way: at each step in the iteration a new candidate is proposed through a stochastic mechanism. Our implementation of these algorithms is through the SciPy package in python. [137] For both algorithms, we must specify a candidate solution that will be iteratively improved upon. To better search the space, we choose 1000 random initial conditions, and run the algorithms separately for each. That is, each hyperfine component is chosen randomly according the above constraint (i.e. $\leq |0.5|$). This also serves to reduce any potential bias that could cause the algorithm to get stuck on a local optimum. To further improve this process, we iterate each initial condition in the following way: when a solution is found, we then use this as the initial condition for the next run, repeating 10 times. All other parameters of the optimization algorithms are set to their default values. Finally, we use the Earth's magnetic field, i.e., 50 $\mu$ T It must also be noted that the differential evolution algorithm seeks to *minimize* an objective function (i.e. optimality in our case). This can easily be modified to find the maximum by returning the negative of our objective function.

## 4.3 Optimal 10RP

To demonstrate the utility of the method described above, we will first examine the case of a 10RP to see whether a needle is possible. A similar approach was done using the anisotropy metric, [17] which does not reflect the spread in the distribution and therefore is unlikely to find the desired parameters. Furthermore, the hyperfine-parameters found were *smaller*, which is not feasible for Earth-strength fields. [17, 110] The 10RP has also been suggested to perform best [107] and is consistent with radiofrequency experiments. In this case we consider the nuclei to be spin-$\frac{1}{2}$. To run the optimization routine we must specify an initial guess which we choose at random; when we obtain an answer, we then run routine again using *this* solution as our new initial condition. This is repeated until the solution changes by less than 1 %. Finally, this entire process is repeated for 1000 random initial conditions to better search the parameter space.

This process yields numerous different HF-parameters that produce sharp features in the yield with similar values for optimality – i.e., the solution is not unique. Here we showcase one in particular which bears resemblance to flavin: A = diag(-0.242, -0.283, 0.286) mT, shown in Fig. 4.1. This solution was found through both Nelder-Mead and differential evolution, suggesting that it is the global optimum. Although the width of this peak is considerably larger (i.e. less sensitive), the lifetime of the radical pair is significantly shorter. In addition, the 'anisotropy' of this yield is larger. This unequivocally demonstrates that it is possible to obtain a needle with a 10RP. Furthermore, although it persists for shorter lifetimes, albeit with degradation, whereas the flavin-trp completely disappears for lifetimes less than 10$\mu$s.

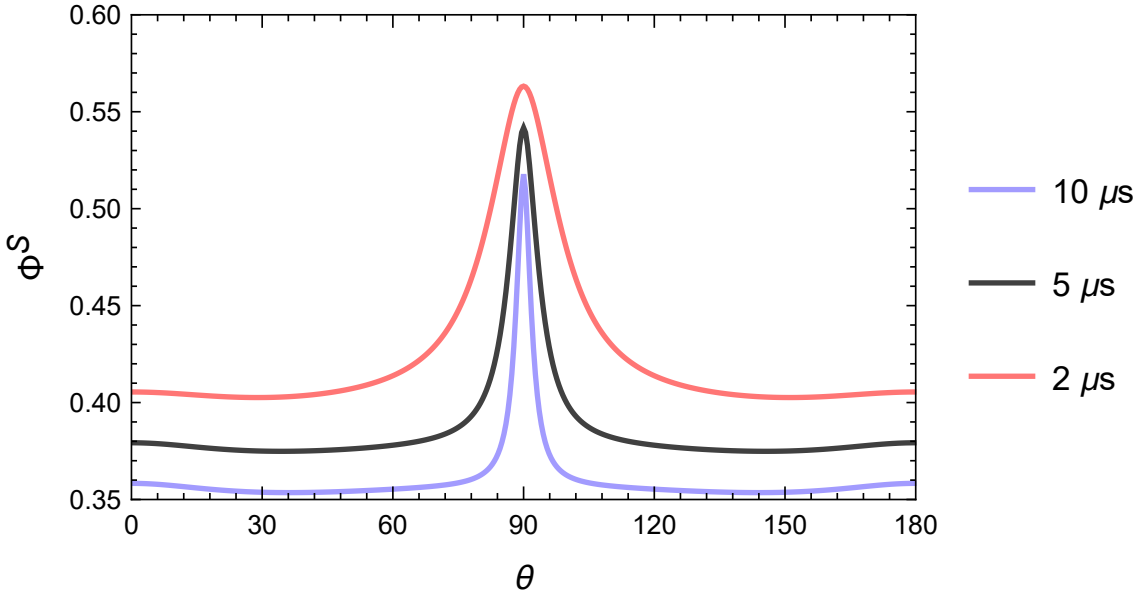


Figure 4.1: Singlet yield for a 10RP with spin-$\frac{1}{2}$ nuclei, hyperfine tensor diag(-0.242, -0.283, 0.286) mT, and Earth-strength magnetic field (0.05mT). For clarity, these figures have been offset by (0, 0.02, 0.04).

## 4.4 Optimal flavin partner

In this section we apply the same methodology, but instead use a flavin-based RP and find the partner radical that maximizes the optimality. First we will use the parameters from [41] and only change the HFI of the partner radical. In this way we can see which HFI provides the best signal, and more importantly how close a tryptophan partner is to this.

## 4.5 Flavin Based Radical Pair with Spin One-Half Partner

In this section we consider the optimal partner to flavin, first considering the case of a spin-$\frac{1}{2}$ nuclei. This radical is actually quite similar to trp, suggesting that Trp is indeed optimal.

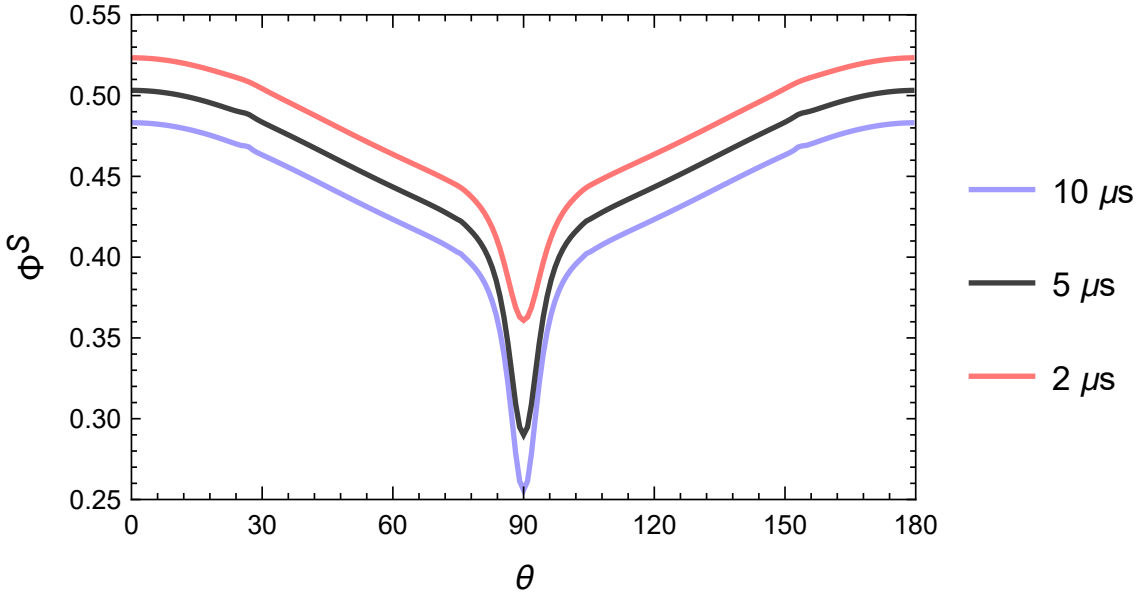


Figure 4.2: Singlet yield for a flavin based 11RP with spin-$\frac{1}{2}$ nuclei, HF tensor diag(0.0066, -0.00050, 1.92980) mT, and Earth-strength magnetic field (i.e. 0.05mT). (A) Lifetime of radical-pair is 10 $\mu$s, (B) Lifetime of radical-pair is 2 $\mu$s. These figures have been offset by (0, 0, 0).

Although this one appears to persist for shorter times – this is consistent with our initial calculations that showed a small perturbation in the HFI led to robustness to variations in the decay rate.

The origin of this improvement is the *reduction* of the avoided crossing distance. This is because the smaller the distance, the more ST-interconversion. Furthermore, the values outside of this are simultaneously large, so that the mixing is low there, and therefore the singlet is maximized. In other words there are two effects occuring: we want the avoided crossing distance to be very small, but also, the distance at other values to be very large. IN this we only have appreciable ST-interconversion at a small range of values near the avoided crossing, leading to a needle. So really what we want to compare is the difference between the avoided crossings at 90 degrees and zero – the larger this is, the more pronounced the needle will be. Consequently, the angle of approahc also matters, with larger angles leading

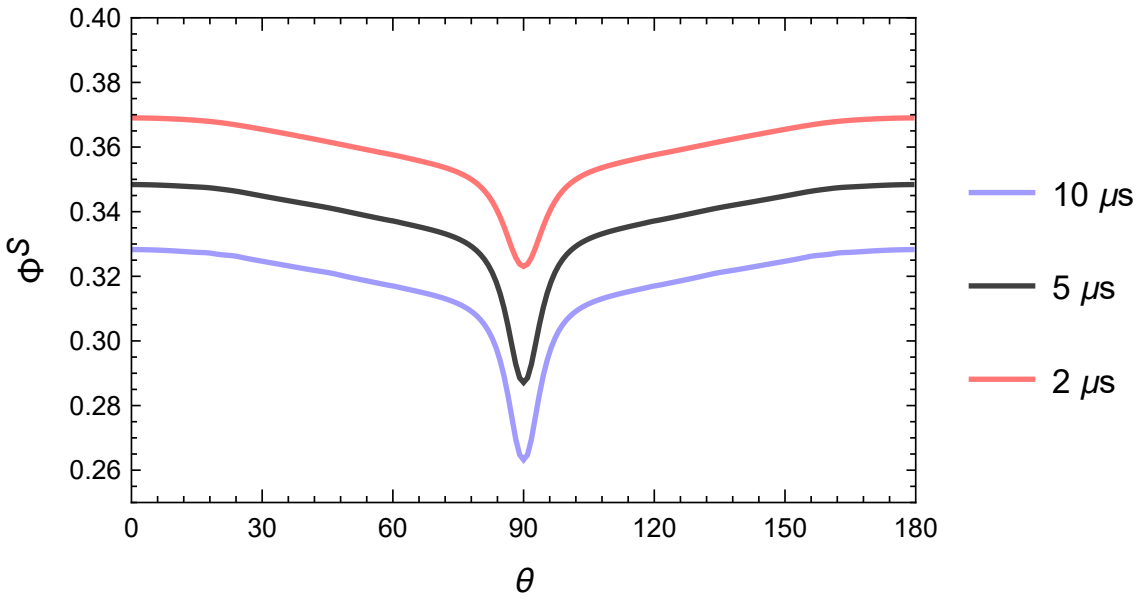


Figure 4.3: Singlet yield for a flavin based 11RP with spin-1 nuclei, HF tensor diag(1.1630, 1.2504, -0.0407) mT, and Earth-strength magnetic field (i.e. 0.05mT). (A) Lifetime of radical-pair is 10 $\mu$s, (B) Lifetime of radical-pair is 2 $\mu$s

to a higher directional sensitivity of the yield.

## 4.6 Optimal 11RP

In this section we now consider the case of a 11RP that is *not* flavin-based. Although the flavin-trp based radical-pair displays a needle, the lifetime needed ( 100 $\mu$ s) is implausibly long. Therefore, we want to find a partner radical that still mains an appreciable peak, but for shorter lifetimes.

To determine whether there exists a set of HF parameters that produce a needle-like feature for longer lifetimes we let B = 0.05 mT, k = (1/2) MHz, and the spin of the flavin partner radical be $\frac{1}{2}$. Applying our routine to find the optimal HFI gives the diagonal matrix (0.014, -0.00045, 1.63) mT gives the following yield: these calculations demonstrate that from the

perspective of the singlet-yield, a flavin-trp based radical pair is not the only one capable of producing a 'needle'.

## 4.7 Conclusion

At present it is not clear how these HF parameters could be realized biologically. However, they do provide a useful benchmark with which to measure the actual magnetoreceptor. In this way, we find that a RP based on flavin performs remarkably well, supporting the idea that it is indeed optimized. However, it must be kept in mind that these solutions are not guaranteed to be optimal. It is outside the scope of this work, but the flexibility offered by the constrained optimization approach above could be used to ask, e.g., the optimal number of nuclei, and their spins, by constraining them to be less than a feasible number (e.g. 20 and 5, respectively). The calculations also suggest that the partner radical to flavin is a spin-1/2 nuclei, consistent with the proposal of the hydrogen nuclei from tryptophan.

# Chapter 5

# Biphasic response of flavin to light-intensity.

Experiments with European Robins have shown that light-intensity within some 'functional window' is required for their magnetic compass to function properly – light-intensities that are too high (or low) cause the bird to become disoriented. In addition, many birds, particularly European Robins, are night-migratory. [6, 58] In this chapter we suggest that both of these effects can be understood through flavin's photocycle. In particular, its signaling state (i.e. semi-reduced flavin) is known to be simultaneously activated, and deactivated, by light through different redox reactions. This antagonistic effect of light-intensity produces a biphasic response in the equilibrium signaling state concentration of flavin with respect to light-intensity. This characteristic is suggested to underlie the experimentally observed functional window – i.e. light-intensities above (or below) some threshold will not activate enough cryptochrome receptors, and therefore lead to disorientation. Furthermore, the low-light levels experienced during night-migration pose a difficulty for understanding the functioning of a light-dependent magnetic compass. It is shown that when the light-intensity which produces the maximum signaling state concentration is decreased, the maximal concentration

correspondingly increases, suggesting that this system performs better under low-light conditions, thereby providing a possible explanation for night-migration. To better illustrate these results, we couple the photocycle to a previously developed signal transduction mechanism to calculate signal-to-noise ratios for various system parameters.

## 5.1 Background

Since the initial investigations of magnetoreception, it has been well known that the ambient light source plays a crucial role. Consequently, numerous photoreceptor based mechanisms have been proposed. [45, 46, 110] However, the interplay between light and magnetic field effects remains poorly understood, largely due to the complex nature of the behavioral responses observed. [157] As discussed earlier, short-wavelength light is required for the avian magnetic compass to function properly, and this can be understood straightforwardly through the absorption spectrum of cryptochrome. Although the effects of wavelength can be easily understood, an understanding of the light-intensity effects so far have remained elusive. Indeed, the nature of responses at higher light-intensities include disorientation (i.e. random orientations), but also 'fixed-responses'. [125, 149, 144] These fixed-responses remain the same despite changes in environmental stimuli. Their origin, and relevance, are unclear, although they have been suggested to be due to a compass based on magnetite.

Conceptually, the intensity of a light source can be understood as the number of photons it contains. While the wavelength of the light source characterizes whether a molecule will be activated, the intensity describes how many of them will be activated. From this, it might be expected that higher light-intensities will activate more receptors, and therefore lead to a better signal-to-noise ratio (or directional precision). However, experimentally it is found that monochromatic light above approximately 0.016 $\frac{\mu\text{mol}}{\text{s m}^2}$ leads to disorientation, and similarly for sufficiently low light-intensities. This cutoff appears conserved across different

species, suggesting that it is a characteristic of the receptor molecule. [49] In other words, light-intensities within some 'functional window' are required to observe proper orientation. One way we can understand this is by having two processes that depend on light-intensity – one which activates cryptochrome, and one which deactivates it. These opposing processes will overlap in some region of light-intensities where their effects are comparable, and lead to maximal response. Outside of this, one of the processes will dominate, leading to a rise (from the activation process), followed by a fall (from the deactivation process). Indeed, this is the case for cryptochrome, whereby light simultaneously causes it to enter its signalling state, and also transition out of it.

In addition to the functional-window characteristic of light-intensity, it is also well known that many birds migrate at night, particularly European Robins which remain the best studied organism for magnetoreception. [147] However, it remains a considerable challenge to understand how their light-dependent magnetic compass operates under these low-light conditions. [82, 39] Indeed, this is also likely when its functioning is more critical, i.e. under cloud cover when other cues are unavailable. Furthermore, sea turtles have been shown to possess a magnetic compass. Similarly, their environment, i.e. murky waters, often contains low light levels. [74] These observations suggest that cryptochrome must be able to operate in low-light conditions.

Indeed, *Arabidopsis Cryptochrome* 2 performs better under low-light conditions, albeit for an entirely different reason. In this case, light activation causes *AtCry2* to become quickly degraded; [1] the subsequent regeneration occurs on a smaller timescale. Therefore, in the presence of high light-intensities, most of the molecules will be degraded and unable to receive further signals. In contrast, low-light conditions will activate a relatively smaller fraction of the molecules, allowing others to continue to absorb light, thereby performing better. However, this mechanism is not expected to underlie the effects observed in the avian magnetic compass, as its signaling state monotonically decreases with increasing light

intensities, and does not display a functional window. [1, 136]

Furthermore, experimental evidence suggests that brain-regions linked to processing magnetic information, i.e. Cluster N, are highly active at night. [37, 83, 166] In addition, these regions show low neuronal activity during the day, suggesting that the light-dependent magnetic compass may *only* be used during night-time. [166] If the avian magnetic compass is indeed the most precise compass available, [41] this would suggest night-migration is favorable over daytime migration. However, numerous factors drive the decision to migrate at night, e.g., predator avoidance, and air conditions, precluding a straight-forward explanation. [6] Finally, some species migrate both during the day and night, e.g., the meadow pit (*Anthus pratensis*). [166] In this chapter we show, qualitatively, that the aforementioned effects of light-intensity can be understood through cryptochrome's photocycle.

## 5.2 Flavin photocycle

A proposed photocycle for *Arabidopsis Thaliana* cryptochrome is shown in Fig. 5.1. [15, 105] In this thesis we also assume that it describes the photocycle for European robin's cryptochrome. In the absence of light, flavin will exist in its oxidized form ($FAD_{ox}$), i.e., its initial state. [3] Upon absorption of light, $FAD_{ox}$ accepts an electron from a nearby chain of tryptophan residues on cryptochrome (not shown), [8] resulting in a radical pair between the now semi-reduced flavin ($FADH^{\bullet}$) and tryptophan. This radical-pair can revert back to the ground state of flavin through recombination, with rate-constant ($k_{1b}$), but only while in the singlet state. As described previously, an external magnetic-field will cause this radical-pair to interconvert between its singlet and triplet states, thereby slowing this back-reaction down by causing it to enter the non-reactive triplet state. Therefore, it is expected that this back reaction (described by $k_{1b}$) is decreased in response to a magnetic field, consistent with experiment. [142, 104] Therefore, we model the effects of the magnetic field as slowing down

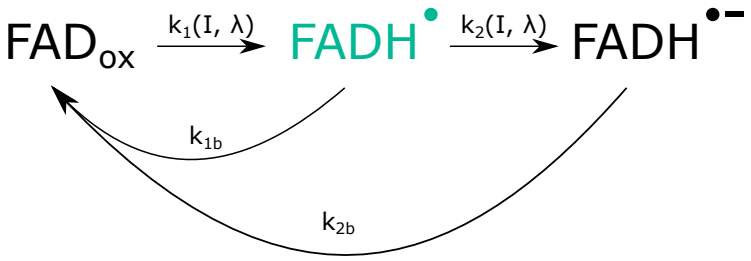


Figure 5.1: Flavin photocycle showing the light-dependent $(k_1, k_2)$, and independent $(k_{1b}, k_{2b})$, reactions; $k_{1b}$ depends on the strength and/or orientation of ambient magnetic field. The semi-reduced state is highlighted in green to indicate that it is the biologically active (i.e. signaling) state.

the rate-constant $k_{1b}$ by a constant factor, e.g. 10 %.

The electron transfer that leads to the formation of semi-reduced flavin causes a structural re-arrangement from electrostatic effects. In particular, while in this state, cryptochrome's C-terminal domain unfolds, enabling, e.g., protein partners to bind. [96, 59] This process is poorly understood, with suggestions including direct binding to a potassium-gated voltage-channel, [164] interaction with proteins linked to glutamate reception, [42] and catalyzing the phosphorylation of a kinase protein. [103] In the first two cases, the signal transduction process interacts directly with proteins that affect the membrane potential and signal transmission, respectively. In the last case, kinase binding could catalyze its phosphorylation; upon unbinding, this now activated kinase can then phosphorylate another protein, thereby propagating the signaling cascade.

The semi-reduced state can be further reduced through light-absorption to form the fully-reduced state ($FADH^{\bullet-}$), which is biologically inactive. This state re-oxidizes through a light (and magnetic) independent process back to the ground state, described by the rate-constant $k_{2b}$. The absorption spectra for the oxidized and semi-reduced forms of flavin are shown in Fig. 5.2 where it can be seen that the semi-reduced spectra is red-shifted with respect to the oxidized form, enabling it to now absorb green light.

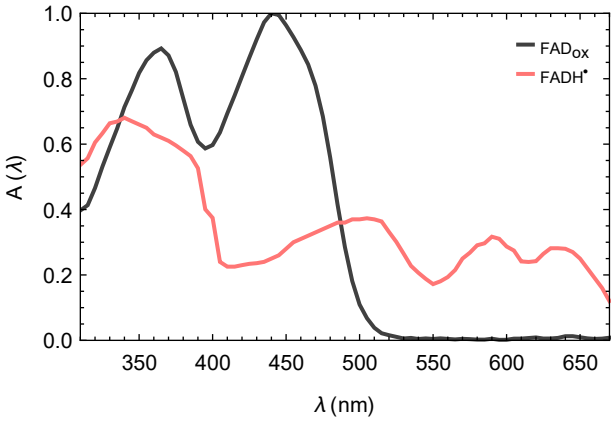


Figure 5.2: Absorption spectra for the oxidized (black curve) and semi-reduced (red curve) forms of flavin.

Although light activates cryptochrome by converting flavin to its semi-reduced signaling state, it also deactivates it by converting the semi-reduced state to the fully-reduced one, thereby displaying an antagonistic effect. Experiments have shown that in the presence of short-wavelength (e.g. blue) and also yellow light, birds are disoriented – this can be understood, e.g., through cryptochrome's photocycle whereby yellow light deactivates cryptochrome, displaying an antagonistic effect to blue-light. Furthermore, this antagonistic effect leads to a biphasic response to light intensity. This can be understood as follows – for sufficiently small intensities, the re-oxidation reactions will dominate, leading to a small accumulation of the signalling state. Increasing the light intensity will begin to favor the semi-reduced state as it out-competes re-oxidation; however, for sufficiently high light intensities the forward reactions will occur much faster than the back, leading to an accumulation in the fully-reduced state. In other words, increasing the light-intensity initially leads to more concentration in the signaling state, but at some point this effect is reversed, leading to a decrease, i.e., a biphasic response.

We will now describe this effect quantitatively by modeling the photocycle assuming all reactions can be described through action first order processes. The equations describing

this system are:

$$\frac{\mathrm{d}[\mathrm{FAD_{ox}}]}{\mathrm{d}t} = -k_1[\mathrm{FAD_{ox}}] + k_{1\mathrm{b}}[\mathrm{FADH^{\bullet}}] + k_{2\mathrm{b}}[\mathrm{FADH^{\bullet -}}] \tag{5.1a}$$

$$\frac{\mathrm{d}[\mathrm{FADH^{\bullet}}]}{\mathrm{d}t} = k_1[\mathrm{FAD}] - (k_{1\mathrm{b}} + k_2)[\mathrm{FADH^{\bullet}}] \tag{5.1b}$$

$$\frac{\mathrm{d}[\mathrm{FADH^{\bullet -}}]}{\mathrm{d}t} = k_2[\mathrm{FADH^{\bullet}}] - k_{2\mathrm{b}}[\mathrm{FADH^{\bullet -}}] \tag{5.1c}$$

Adding the equations in (5.1), integrating, and assuming that initially all of the flavin are in their ground state (i.e. $[\mathrm{FADH^{\bullet}}](0) = [\mathrm{FADH^{\bullet -}}](0) = 0$) gives the conservation equation ($[\mathrm{FAD}](t) + [\mathrm{FADH^{\bullet}}](t) + [\mathrm{FADH^{\bullet -}}](t) = [\mathrm{FAD_{ox}}](0)$) which reflects the fact that flavin is only transformed through this process so that the total amount of flavin in the various redox states summed together is equal to the initial concentration.

The light-dependent rates, $k_1$ and $k_2$, can be calculated from first-principles as: [81]

$$k_i = 2.303\epsilon_i(\lambda) l \phi_i(\lambda) I \equiv \sigma_i I \tag{5.2}$$

where the subscript 'i' is one or two for the oxidized and semi-reduced states of flavin respectively. Further, $\epsilon_i$ denotes the molar-extinction coeffcient, which measures how strongly light is absorbed at a given wavelength, $l$ is the path-length of the sample, $\phi_i$ is the quantum yield which captures the effect that not *all* molecules that absorb light undergo the reaction of interest – there is a 'loss' due to competing reactions (e.g. fluorescence, internal conversion). This value is often less than unity, but can be larger in cases where there is amplification. Lastly, $I$ is the irradiance of the ambient light source. Finally, since we are focused on the intensity dependence of this rate, we define $c_i$ in the second relation. Therefore, the photoconversion cross-section, $\sigma$ measures how well light initiates the reaction of interest and is composed of two processes: (1) first, light must be absorbed, which is measured by the extinction coefficient, and (2) once the light is absorbed, it must lead to the reaction of interest, competing with, e.g., relaxation, etc. as measured by the quantum yield

The dynamics of this system are fast on a biological timescale (i.e. obscured by diffusion) allowing us to focus on its equilibrium state. Setting the above equations, Eq. (5.1), equal to zero, we can solve for the equilibrium concentrations:

$$[\mathrm{FAD}_{\mathrm{eq}}](I, MFE) = \frac{(k_{1\mathrm{b}}(1-\mathrm{MFE}) + \sigma_2 I)k_{2\mathrm{b}}N_{\mathrm{Cry}}}{k_{1\mathrm{b}}(1-\mathrm{MFE})k_{2\mathrm{b}} + k_{2\mathrm{b}}(\sigma_1+\sigma_2)I + \sigma_1\sigma_2 I^2} \tag{5.3a}$$

$$[\mathrm{FADH}^{\bullet}_{\mathrm{eq}}](I, MFE) = \frac{k_{2\mathrm{b}}N_{\mathrm{Cry}}\sigma_1 I}{k_{1\mathrm{b}}(1-\mathrm{MFE})k_{2\mathrm{b}} + k_{2\mathrm{b}}(\sigma_1+\sigma_2)I + \sigma_1\sigma_2 I^2} \tag{5.3b}$$

$$[\mathrm{FADH}^{\bullet-}_{\mathrm{eq}}](I, MFE) = \frac{N_{\mathrm{Cry}}\sigma_1\sigma_2 I^2}{k_{2\mathrm{b}}k_{1\mathrm{b}}(1-\mathrm{MFE}) + k_{2\mathrm{b}}(\sigma_1+\sigma_2)I + \sigma_1\sigma_2 I^2} \tag{5.3c}$$

The oxidized state monotonically decreases with respect to light-intensity. This is consistent, e.g., with hypocotyl length [136]. In contrast, the light-effects on the avian compass is biphasic. In order to have a biphasic response with respect to intensity, there must exist an extremum in the equilibrium concentration. We will investigate each redox-state in turn by taking the derivative with respect to intensity, setting it to zero, and solving for the intensity to determine if this occurs at an allowable value (N.B. these equations being second order have two solutions; only the positive ones are taken as candidates):

$$I_{\mathrm{opt}_{\mathrm{FAD}}} = \frac{-k_{1\mathrm{b}}(1-\mathrm{MFE}) \pm \sqrt{-k_{1\mathrm{b}}(1-\mathrm{MFE})(k_{2\mathrm{b}} - k_{1\mathrm{b}}(1-\mathrm{MFE}))}}{\sigma 2} \tag{5.4a}$$

$$I_{\mathrm{opt}_{\mathrm{FADH}^{\bullet}}} = \sqrt{\frac{k_{2\mathrm{b}}k_{1\mathrm{b}}(1-\mathrm{MFE})}{\sigma_1\sigma_2}} \tag{5.4b}$$

$$I_{\mathrm{opt}_{\mathrm{FADH}^{\bullet-}}} = 0 \tag{5.4c}$$

Looking at Eq. (5.4a), we see that in order to have the maximum occur at a positive intensity requires the numerator to be positive. Simplifying this expression shows that this only occurs under conditions that are not physically-realizable (i.e. negative rate-constants and/or photo-conversion cross-section). Therefore, in terms of the light-intensity effects, the oxidized state cannot be the signaling state. However, looking at (5.3a), it can be seen that the oxidized concentration monotonically decreases with respect to light-intensity. In

Arabidopsis, it has been shown that the hypocotyl length is inversely proportional to the light-intensity, suggesting that the oxidized state could mediate hypocotyl elongation [136]. Similarly, it can be seen that the fully-reduced state does not display an extremum for *any* set of parameters, thereby ruling it out as a candidate signalint state.

Finally, it can be seen from (5.4b) that any physically-realizable parameters will lead to an optimal intensity that is possible, thereby providing a biphasic response. For *Arabidopsis Thaliana* 2, this state has been suggested as the signaling state, albeit on different grounds. [10] Now that we have established there is an optimal intensity for the signalling state, we can investigate how its location affects the signaling-state equilibrium concentration. Without loss of generality, we can solve (5.4b) for $k_{1\mathrm{b}}$ and plug this into (5.3b) to obtain

$$[\mathrm{FADH}^{\bullet}_{\mathrm{eq}}](I_{\mathrm{opt}}) = \frac{k_{2\mathrm{b}}\sigma_1 N_{\mathrm{Cry}}}{k_{2\mathrm{b}}(\sigma_1+\sigma_2) + 2\sigma_1\sigma_2 I_{\mathrm{opt}}} \tag{5.5}$$

This shows that as we shift the location of optimal intensity to the right (i.e. increase $I_{\mathrm{opt}}$), the concentration of signaling-state available is correspondingly decreased. In other words, this system performs better under lower light-intensities, consistent with the observation that European robins migrate at night. [83] To illustrate this point better, we plot Eq. 5.5 in Fig. 5.3 for various optimal-intensity values for *AtCry1* and *AtCry2*. Here we clearly see that when we want our system to respond maximally for higher light-intensities, there is a corresponding decrease in the peak signaling concentration, and also a broadening. This broadening implies that the system becomes less sensitive to light-intensity In addition, this effect will be wavelength-dependent through $c_1$ and $c_2$.

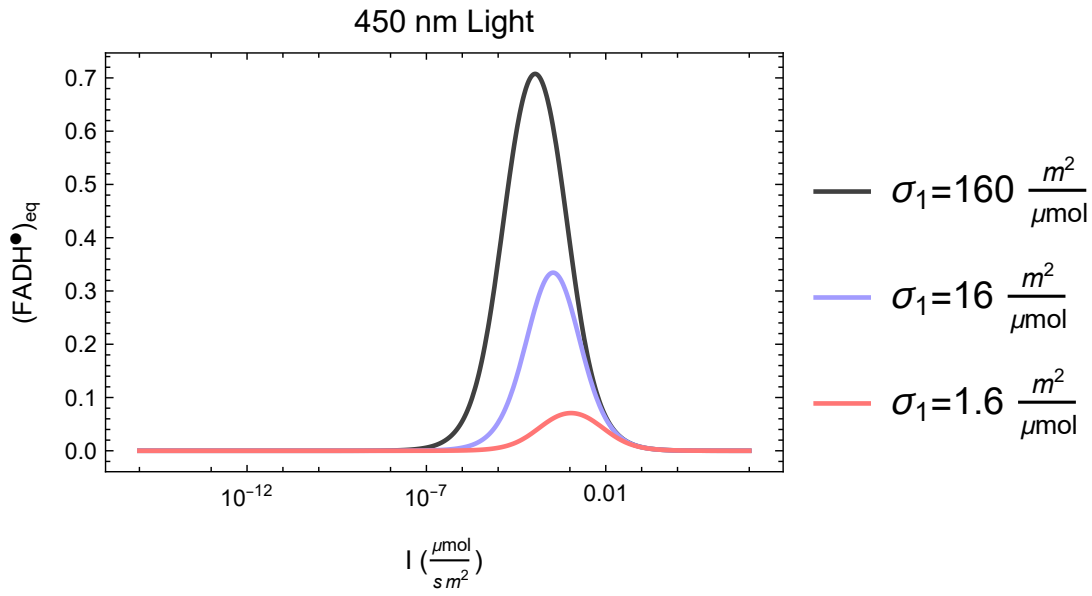


Figure 5.3: Equilibrium concentration of the semi-reduced flavin state as a function of light-intensity. This demonstrates that there is a peak, and that the functional window of magnetoreception can be understood from the biphasic response. Furthermore, it is seen that when the peak is shifted to the left (by changing $\sigma_1$), the maximum correspondingly increases, suggesting that a flavin based magnetic compass operates better under lower light intensities.

## 5.3 Weaver Model of Signal Transduction

To better illustrate the results in the last section, we will combine the photocycle with a previously described signal transduction mechanism, [140] which we briefly describe. The Weaver model shown in Fig. 5.4 consists of: (1) a cell that produces a ligand at a rate which is magnetically-senitive, (2) a nearby neuron with extracellular receptors that bind the ligand, and (3) a mechanism to remove the ligand (e.g. through passive diffusion). In this way, the equilibrium concentration of the ligand, and therefore the number of ligand-bound receptors (which constitutes the signal), will depend on the magnetic-field. An increase in the magnetic-field will result in a faster rate of ligand production, and therefore a higher number of bound receptors, which is assumed to be the signal. Competing with this binding process are effects due to stochastic noise. Summarising, the Weaver model describes how a cell transduces magnetic stimuli to a chemical signal which is received by another cell,

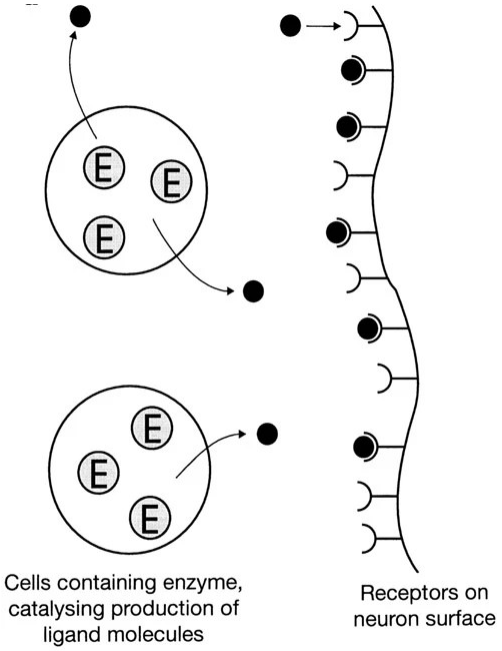


Figure 5.4: Weaver model of signal transduction [140] containing: cells producing ligand through a magnetically-sensitive process, and nearby nueron with receptors that bind this ligand.

thereby completing the signal transduction.

The reactions in Fig. 5.4 are:

$$\mathrm{E} + \mathrm{S} \xrightarrow{\mathrm{k(B)}} \mathrm{L} \tag{5.6a}$$

$$\mathrm{L} + \mathrm{R} \xrightarrow{\mathrm{k}_f} \mathrm{C} \tag{5.6b}$$

$$\mathrm{C} \xrightarrow{\mathrm{k}_r} \mathrm{L} + \mathrm{R} \tag{5.6c}$$

$$\mathrm{L} \xrightarrow{\mathrm{k}_p} 0 \tag{5.6d}$$

where E is the enzyme catalyzing the reaction, S is the substrate, L is the ligand, R is the (unbound) receptor and C is the amount of bound receptors (complexes). The first equation describes the ligand production from the substrate, the second and third describe the binding and dissociation of the ligand with the receptor respsectively, while the fourth describes the removal of the ligand described by the rate-constant $k_\mathrm{p}$ (not shown in figure).

If one assumes mass action kinetics for each of these reactions, we have the following system of ODEs (ignoring the enzyme and substrate concentrations which are approximately unchanged):

$$\frac{\mathrm{d}L}{\mathrm{d}t} = k(B)S - k_p L - k_f LR + k_r C \tag{5.7a}$$
$$\frac{\mathrm{d}R}{\mathrm{d}t} = -k_f LR + k_r C \tag{5.7b}$$
$$\frac{\mathrm{d}C}{\mathrm{d}t} = k_f LR - k_r C \tag{5.7c}$$

where it has been assumed that the substrate concentration is sufficiently low, so that the ligand-production varies linearly with substrate. Adding equations 5.7b and 5.7c and integrating gives the conservation equation $R(t) + C(t) = R(0) + C(0) \equiv R_{\mathrm{T}}$ which reflects the fact that the total number of receptors (i.e. bound + unbound), $R_{\mathrm{T}}$, remains unchanged. This equation holds for all times, in particular at equilibrium. Assuming the system is in equilibrium, and combining the conservation equation with (5.7c) allows us to solve for the equilibrium concentration of bound receptors (C):

$$C_{\mathrm{eq}} = \frac{R_T}{1 + K_{\mathrm{D}} \frac{1}{L_{\mathrm{eq}}}} \tag{5.8}$$

where the dissociation constant, $K_{\mathrm{D}} \equiv \frac{k_r}{k_f}$, has been introduced.

We can simplify further by introducing the dimensionless parameter, $\tau = kt$ so that $\frac{\mathrm{d}}{\mathrm{d}t} = k\frac{\mathrm{d}}{\mathrm{d}\tau}$. Furthermore, adding (5.7b) and (5.7c) gives a constant so that we can ignore one of them, i.e., (5.7b) since we are concerned with the number of bound receptors:

$$k\frac{\mathrm{d}L}{\mathrm{d}\tau} = kS - k_p L - k_f LR + k_r C \tag{5.9a}$$
$$k\frac{\mathrm{d}C}{\mathrm{d}\tau} = k_f LR - k_r C \tag{5.9b}$$

Adding (5.9a) and (5.9b) and dividing by $k_p$ gives $\frac{k}{k_p}\frac{\mathrm{d}(L+C)}{\mathrm{d}\tau} = \frac{k}{k_p}S - L$; now applying the

assumption that k << $k_p$ allows us to ignore the left-hand side and obtain $L = \frac{k}{k_p}S$. The $\frac{k}{k_p}S$ term cannot be ignored since S could be large. Equation (5.8) shows how the number of bound receptors (i.e. the signal) at equilibirum depends on the MF through the ligand concentration. The Weaver model takes $C_{eq}$ as its signal, and compares the signal produce in the presence and absence of the GMF, i.e., $S = C_{eq}(B = 0.5G) - C_{eq}(B = 0)$. Lastly, the Weaver model considers noise due to the stochastic fluctuations of binding, given by Eq. 5.10 Combining these two equations allows the calculation of the signal to noise ratio.

The spin-dynamics and photocycle previously described can be combined with a signal transduction model to investigate the effect of model-parameters on magnetic field effects (MFEs) as measured by the signal to noise ratio (SNR) The noise is taken to be stochastic fluctuations about the average number of bound receptors:

$$N \equiv \delta C_{\mathrm{op}} \approx \sqrt{\frac{q_{\mathrm{op}}}{(1+q_{\mathrm{op}})^2} R_{\mathrm{T}}} \tag{5.10}$$

## 5.4 Combining Cryptochrome's Photocycle With Weaver Model of Signal Transduction

With the Weaver model and flavin photocycle introduced, we now combine them. It is assumed that while in the signaling state (i.e. semi-reduced flavin) a ligand is produced through a cascade of events (beginning, e.g., with phosphorylation) described as a first-order process, shown in Fig. 5.5. The rate this occurs is magnetically-sensitive, as can be seen in Eq. 5.3, owing to the fact that the equilibrium concentration of semi-reduced flavin (which is proportional to the ligand production rate) is magnetic-dependent. This is in contrast to the Weaver model, where it was assumed that the rate-constant itself was magnetic-dependent. Other than this, everything else remains the same, allowing us to use the equations with no

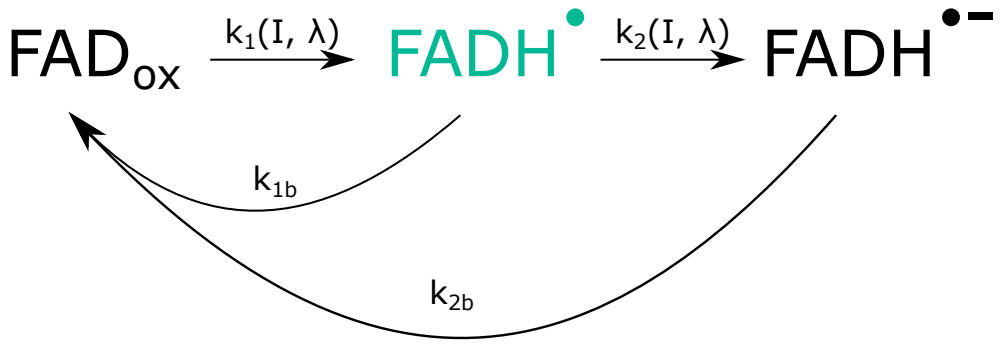


Figure 5.5: Cryptochrome's photocycle combined with the Weaver model of signal transduction. While in the semi-reduced state (colored green), cryptochrome is biologically active, undergoing a molecular binding event (e.g. phosphorylation) which leads to the production of a ligand. This ligand binds to extracellular receptors on a nearby neuron, thereby completing the signal transduction step.

modification. Weaver's substrate concentration corresponds to our semi-reduced state, i.e., $S = \mathrm{FADH}^{\bullet-}_{\mathrm{eq}}$ so that our ligand concentration is $L = \frac{k}{k_{\mathrm{p}}}\mathrm{FADH}^{\bullet-}_{\mathrm{eq}}$. Substituting into (5.8), and calculating the signal according to $S = C(B) - C(0)$ gives for the signal:

To calculate the signal to noise ratio, the following parameters are used: the rate at which the ligand is produced is $k_{\mathrm{L}} = 10^3$, the rate at which the ligand is degraded is: $k_{\mathrm{L}} = 10^4$, and the dissociation constant is $k_{\mathrm{D}} = 10^{-8}$, chosen as in Weaver [140] so that the response time is on the order of milliseconds, i.e., sufficiently fast for magnetic sensing. Furthermore, the number of receptors is chosen as $R_{\mathrm{T}} = 10^6$, the rate $k_{1\mathrm{b}}$ is assumed to decrease by 20% in the presence of a magnetic field, and finally the number of cryptochromes is varied over four orders of magnitude. The result of this can be seen in Fig. 5.6 where it can be seen that increasing the number of cryptochromes causes the optimal light intensity to be decreased. In other words, to detect lower light intensities requires more receptors. Furthermore, the optimal light intensity for $10^4$ crpyotchromes occurs at a light intensity (i.e. approximately $10^{-8}\frac{\mu\mathrm{mol}}{\mathrm{s\ m^2}}$) which is consistent with night-migration. [6, 143] This suggests a mechanism whereby the avian magnetic compass can function both during the day and night, i.e., by periodically varying the number of cryptochromes present. Recently it has been argued that

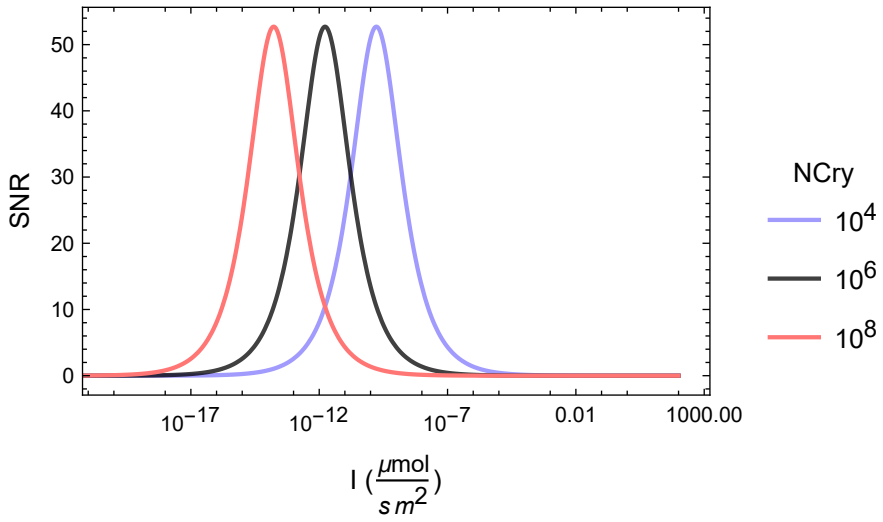


Figure 5.6: Signal to noise ratio as a function of light-intensity for various cryptochrome concentrations. Here it is seen that the optimal light intensity decreases as the number of cryptochrome is increased, suggesting that by varying this concentration, the magnetic compass can function during both the day and night.

the cryptochrome responsible for magnetoreception must be expressed stably throughout the day, as any variation indicates a role in circadian rhythms instead. [165, 164]. These calculations suggest the opposite, that the cryptochrome responsible for magnetoreception is varied throughout the day.

## 5.5 Discussion

In this chapter we have presented model calculations which couple cryptochrome's photocycle with a previously established signal transduction model. [106, 140] In particular, we have shown that he functional window observed during behavioral experiments [143] can be understood through cryptochrome's photocycle. In the flavin photocycle it is not jsut the antagonistic effect that produces the biphasic response, bu rather the interplay between all four rate-constants. Setting $k_{2b}$ equal to zero shows that all flavins will eventually accumulate to the fully reduced – for any light intensity. Furthermore, Eq. (5.4b) shows that setting

$k_{1b}$ equal to zero will put the optimal light-intensity at zero. Strictly speaking a biphasic response will still be present, but would require negative light-intensities. Furthermore, it is found that when the optimal light-intensity location is reduced, the peak of this curve correspondingly gets larger. This suggests that cryptochrome operates *better* under low-light conditions, providing an explanation for the observation that bird migration is often at nighttime. [6, 58] The model developed above is fairly general, and could include, e.g., the case of a cell producing a ligand that binds to extracellular receptors on a nearby neuron. It could also describe molecular processes, e.g., the signalling state could catalyze a reaction to produce a ligand which then binds to a nearby protein, where the receptors now play the role of binding sites. Finally, it was shown that when the number of cryptochrome's is increased, the peak shifts to the left. Consequently, by varying the number of receptors throughout the day, the magnetic system can adapt to the light conditions so that it operates both during the night and day. This lifts a significant constraint imposed on cryptochrome, i.e., that it must be expressed stably throughout the day. It has been argued that any cryptochrome whose expression varies is likely involved in regulating circadian rhythms, and not magnetoreception. [164, 165] However, our calculations instead suggest the opposite, that the cryptochrome responsible for magnetoreception *does* vary throughout the day.

# Chapter 6

# Kinetic Modeling of the *Arabidopsis thaliana* Cryptochrome 1 Photocycle in Alternating Light and Magnetic Field Conditions

Cryptochrome's photocycle contains multiple reaction steps that proceed through radical-pair intermediates and are therefore potentially magnetically-sensitive. For example, light-induced electron transfer results in a radical-pair between flavin and a nearby tryptophan amino acid residue. Similarly, the light-independent reoxidation of flavin to its fully oxidized state proceeds through a radical-pair reaction involving an unknown radical partner, with suggestions including superoxide. [89] Initially, it was suggested the flavin-tryptophan radical-pair was magnetically sensitive, [110] however, recent experiments suggest instead the reoxidation step. [142] Using alternating light and magnetic field conditions, it was found that when the magnetic field was applied only during the dark phase (i.e. when the light was off), a magnetic field effect was observed. This suggests that the light-independent

reoxidation is magnetically sensitive. Using a proposed *Arabidopsis thaliana* cryptochrome photocycle, with a phosphorylation binding model as a proxy for the observation of a magnetic field effect, we present calculations which support the reoxidation step as necessarily being magnetically-sensitive. Importantly, this does not rule out the photoreduction step as *also* being magnetically sensitive. Furthermore, it is found that the observation of magnetic field effects under alternating light and magnetic field conditions places constraints on the allowable reoxidation rates, thereby allowing it to be inferred from behavioral experiments. Finally, it is suggested that, in contrast to what was observed experimentally, a magentic field effect is expected even in the scenario where the dark reaction is magnetically sensitive and the magnetic field is only applied during the light. These results provide support for cryptochrome being a magnetoreceptor, and crucially, that the magnetically sensitive reaction is light-independent.

## 6.1 Background

A key challenge in establishing cryptochrome as a magnetoreceptor is identifying which reaction step is magnetically sensitive. [110, 104, 35, 47] To this end, various experiments [104, 35, 142] have been performed using alternating light and magnetic field conditions. This paradigm has been applied to behavioral experiments using European robins, where seasonally appropriate orientation is indicative of a magnetic field effect. Furthermore, it has also been applied to *Arabidopsis thaliana*, where a magnetic field effect is observed, e.g., from its effect on hypocotyl length. [106, 4] The setup consists of alternating the light source between on and off, with three protocols for applying the magnetic field: (1) during the light period only, (2) during the dark period only, and (3) during both the light and dark period, illustrated schematically in Fig. 6.1. In the experiments, and the calculations presented here, a monochromatic light source of 450nm blue light is used. This simplifies the photocycle of

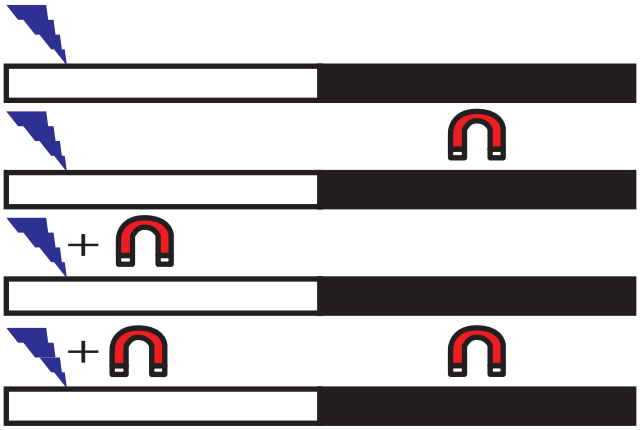

Figure 6.1: The various protocols (light on and then off for all protocols): (a) no magnetic field, (b) magnetic field only during dark (c) magnetic field only during light (d) magnetic field during light and dark.

cryptochrome to a two-state model, shown in Fig. 6.2, as blue-light cannot fully reduce flavin to its fully oxidized state. Experimentally, it was found that when the magnetic field was applied only during the light, no effect was observed. However, when it was applied during only the dark, or during both the light and dark, a magnetic field effect was observed.

To interpret these results, let us first assume that light-dependent flavin reduction (i.e. the forward reaction in Fig. 6.2) is the magnetically sensitive step. In this case, if a magnetic field is only applied during the dark interval, no effect is expected. This is because the magnetically-sensitive reaction is not occurring, and therefore a magnetic field will have no effect. Since a magnetic field effect was observed when it was applied only during the dark, it was concluded that the reoxidation step *must* be magnetically sensitive. [142] However, this does not rule out the possibility that photoreduction is also magnetically sensitive.

If instead it is assumed that reoxidation is magnetically sensitive, the situation becomes more complicated. This is because reoxidaiton is occurring during both the light and dark intervals, so that even if the magnetic field is applied only during the light interval, it can still produce an effect because the magnetically-sensitive reaction step is still occurring. In this case it is difficult to disentangle the effects of light and the magnetic field. This

interplay between the light source and magnetic field complicates the interpretation of the results. In particular, it was found that when the magnetic field was applied only during the light, no effect was observed, which is inconsistent with our previous arguments. That is, if the dark reaction is the magnetically sensitive one, applying a magnetic field only during the light phase should, under the appropriate conditions, produce a magnetic field effect, as magnetically sensitive radical-pairs are still being created. Our calculations suggest the reason for this is the experimental parameters chosen, particularly the length of time for both the light and dark intervals. Indeed, it is found that for sufficiently long light (or dark) intervals, a magnetic field effect is expected. In summary, if the dark reaction (i.e. light-independent) is magnetically sensitive, applying a magnetic field during the light and/or dark is expected to produce an effect (i.e. under all three protocols). Similarly, if the light-dependent reaction is magnetically sensitive, then applying a MF during the dark is not expected to have an effect, while applying it during the light (and also during light and dark), is expected to have an effect. In this chapter we present model calculations based on *Arabidopsis thaliana* cryptochrome which combine its photocycle with a molecular binding event (e.g. phosphorylation) to predict the situations where a magnetic field effect will be observed..

## 6.2 Modeling Cryptochrome Kinetics and Phosphorylation

In the following calculations it is assumed that the effect of the magnetic field is to decrease the rate of the magnetically sensitive reaction step, thereby altering the time spent in the signaling state (i.e. $FADH^{\bullet}$ in Fig. 6.2), or equivalently the steady-state concentrations. In addition, it assumed that while in the signaling state, cryptochrome can undergo phosphorylation due to its c-terminus being exposed, [5, 167, 120, 119] thereby initiating a signal

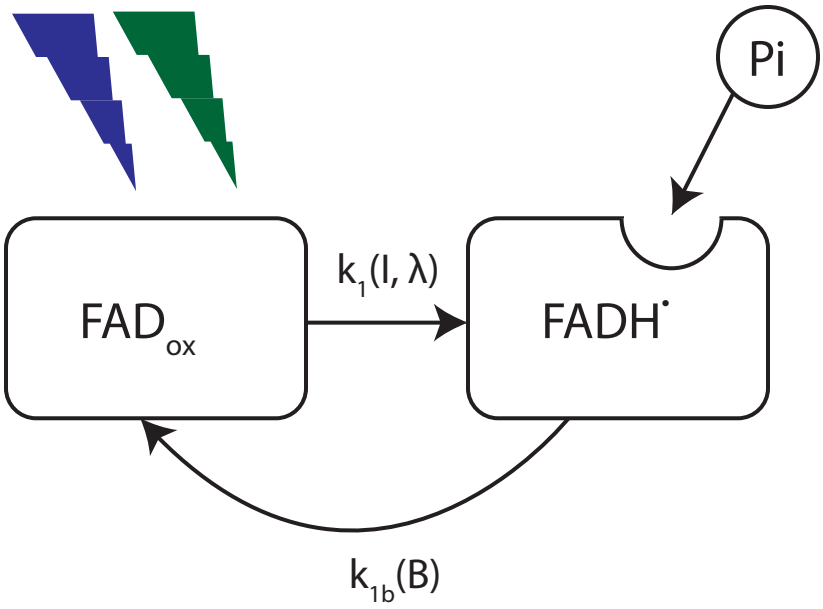


Figure 6.2: Photocycle for AtCry1 showing the light, and magnetic, dependent steps. The initial oxidized flavin is photo-reduced with rate constant $k_1$, triggering a conformational change which leads to phosphorylation. Light independent reoxidation occurs with rate constant $k_{1b}(B)$

transduction cascade. Since the kinase responsible for catalyzing phosphorylation and its dynamics are unknown, we assume a sigmoidal binding process to model phosphorylation. Finally, it assumed that a magnetic field effect (e.g. seasonally appropriate orientation in European robin's or hypocotly length in *Arabidopsis thaliana*) is observed when the fraction of cryptochrome's that are phosphorylated exceeds some threshold, taken here to be 90%.

Assuming the reactions can be described through first order processes, the equations describing the time evolution of the chemical concentrations are given as follows:

$$\frac{\mathrm{d}[\mathrm{FAD_{ox}}]}{\mathrm{d}t} = -k_1(I,\lambda)[\mathrm{FAD_{ox}}] + k_{1b}(B)[\mathrm{FADH^{\bullet}}]$$
$$\frac{\mathrm{d}[\mathrm{FADH^{\bullet}}]}{\mathrm{d}t} = k_1(I,\lambda)[\mathrm{FAD_{ox}}] - k_{1b}(B)[\mathrm{FADH^{\bullet}}]$$

Here, $k_1$ denotes the forward, light-dependent photoreduction rate from $\mathrm{FAD_{ox}}$ to $\mathrm{FADH^{\bullet}}$, and $k_{1b}$ denotes the back reoxidation rate in the dark. In 450 nm blue light, $k_1$ is related to

the photon fluence rate $I_{450}$ (mol m$^{-2}$ s$^{-1}$) as follows: [54]

$$k_1 = \sigma_{450}\, I_{450} = 2.3\, I_{450}\, \epsilon_{450}\, \Phi_{450} \tag{6.2}$$

where $\sigma_{450}$ represents the cross section for photoconversion under 450 nm blue light, which can further be broken down into the product of the molar extinction coefficient $\epsilon_{450}$ and quantum yield $\Phi_{450}$ at 450 nm. The photoconversion cross-section for two-state reduction and reoxidation of AtCry1 was determined to be $\sigma_{450} = 6.4 \times 10^{-5}\ \mu$ mol$^{-1}$ m$^2$. [105] With a fluence rate of 60 $\mu$ mol m$^{-2}s^{-1}$ as used experimentally, [35] this leads to $k_1 = 4.8 \times 10^{-4}$ s$^{-1}$. The reoxidation rate $k_{1b}$ was estimated to be around 0.01 s$^{-1}$ for the two-state photocycle of AtCry1. [105] However, reoxidation rates for phosphorylated AtCry1 are likely to be slower, since the addition of phosphates will hinder the re-folding of the extended C-terminus into its closed form. We will initially assume a reoxidation rate of $k_{1b} = 10^{-3}$ s$^{-1}$ for our calculations and then investigate the effect of changing the reoxidation rate.

As illustrated in Fig. 6.2, we assume that FADH$^\bullet$ is the signaling state triggering the conformational changes in Cryptochrome leading to phosphorylation or other further signaling steps. Because we are interested in the effects relative to the case where there is no magnetic field, we take the difference, and integrate over time of the signaling state. We will refer to this as the accumulated difference, denoted by $\Delta$[FADH$^\bullet$], calculated as:

$$\Delta[\mathrm{FADH}^\bullet] = \int_0^{t_f} (\mathrm{FADH}^\bullet(B) - \mathrm{FADH}^\bullet(B=0))\, \mathrm{d}t. \tag{6.3}$$

This can be understood as the concentration of reaction products that result from phosphorylation in the presence of a magnetic field relative to the case where no field is applied. Finally, the phosphorylation binding dynamics is assumed to follow a logistic curve given

by:

$$p_{bound} = \frac{L}{1 + \exp\big(-k(x - x_o)\big)} \tag{6.4}$$

where $x_o$ sets the midpoint of the curve, L is the maximal value obtained, and k is the 'growth rate' (i.e., steepness of the curve), and x is taken as the accumulated difference defined above. In the following calculations we follow the experimental setup whereby the light was on for 300 seconds, followed by 600 seconds of darkness.

First, let us assume that the forward photoreduction rate (i.e. $k_1$) is magnetically sensitive. Experimentally, [142] a field of $500\mu$T was used; given the size of this field (i.e. $\approx 10\times$ larger than Earth's), we assume $k_1$ decreases by 20% when the field is on. In this case, solving Eq. 6.1 for the three magnetic protocols under alternating light conditions gives the concentrations shown in Fig 6.3. Here it is seen that a magnetic field applied during the dark and not at all are identical, while a magnetic field applied during the light, and during light and dark are identical. Since this contradicts what is observed experimentally, we conclude that photoreduction alone is not sufficient, demonstrating the consistency of our theoretical approach.

Next, let us assume instead *only* the reoxidation reaction rate (i.e. $k_{1b}$) is magnetically sensitive. Using Eq. 6.1 for the three protocols we can calculate the accumulated difference according to Eq. 6.3. The results of both of these calculations can be seen in Fig. 6.4. Finally, using Eq. 6.4 we can calculate the fraction of cryptochrome molecules which are phosphorylated. It is assumed that when this exceeds 90%, a magnetic field effect is observed. In this case, the binding parameters describing phosphorylation are chosen to match the experimental observations, namely that the magnetic field applied during the dark, and during the light and dark, produce a magnetic field effect, while the magnetic field applied only during the light produces no effect. In other words, we impose the following constraints:

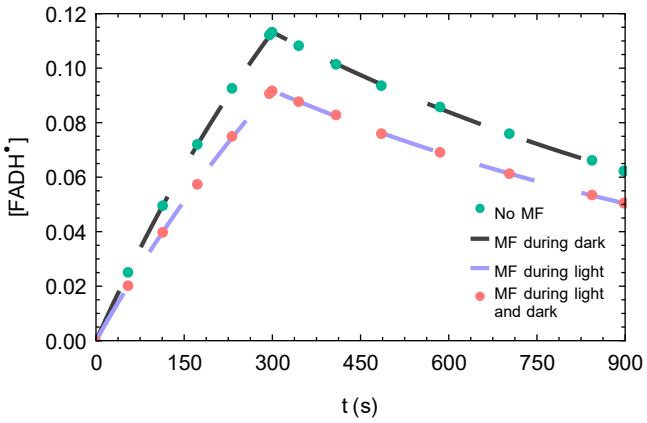


Figure 6.3: Magnetic field effect on the $FADH^{\bullet}$ concentration calculated using Eq. 6.1, assuming that only the forward photo-activation rate $k_1$ is magnetic field dependent. Results are shown for the four experimental protocols described in the legend, with light switched on in the first 300 s, and off in the following 600 s. The parameters were chosen as $k_1 = 4.8 \times 10^{-4}$ s$^{-1}$, $k_{1b} = 10^{-3}$ s$^{-1}$, and the magnetic field was assumed to decrease $k_1$ by 20%

- $p_{bound}$(MF during light) $< 1$ % of maximum.
- $p_{bound}$(MF during dark) $> 90$ % of maximum
- $p_{bound}$(MF during light and dark) $> 90$ % of maximum

which can be satisfied with the following parameters: L = 1, k = 7 and $x_o = 2.6$. The results of these calculations can be seen in Fig. 6.5, demonstrating they are consistent with experimental observation.

However, as argued previously, it is expected that for sufficiently long light (or dark) periods, a magnetic field effect should be observed, as the reoxidation reaction occurs during both. To investigate this further, we now vary the light ($t_{\mathrm{L}}$) and dark ($t_{\mathrm{D}}$) time periods. The results, shown in Fig. 6.6 indeed indicate that for approximately $t_{\mathrm{L}} > 400s$ and $t_{\mathrm{D}} > 1500s$ it is expected that a magnetic field effect will occur in all three protocols.

Finally, to further investigate the effect of system parameters on the observance of a magnetic field effect, we allow the reoxidation rate $k_{1b}$ to vary. First, we fix the dark period at 600s,

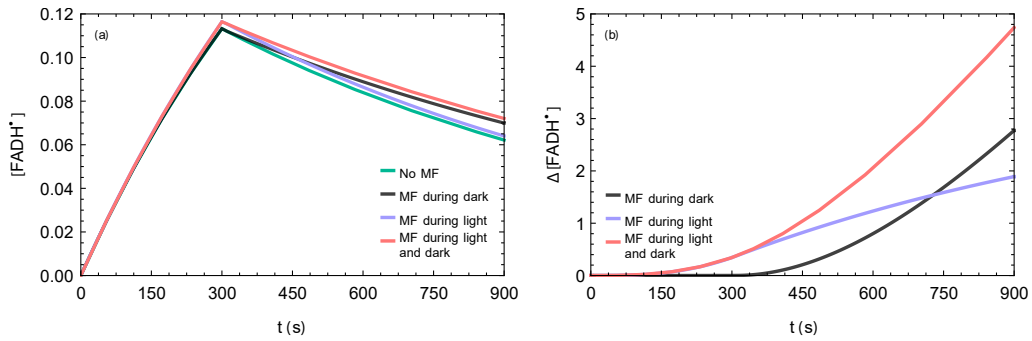


Figure 6.4: (a) In both plots, the decay rates were chosen as $k_1 = 4.8 \times 10^{-4}$ s$^{-1}$ and $k_{1b} = 10^{-3}$ s$^{-1}$, the magnetic field was assumed to only affect the back-reaction, decreasing $k_{1b}$ by 20%. The light was on in the first 300s, and off for the remaining 600s. (a) Magnetic field effect on the FADH$^\bullet$ concentration calculated using Eq. 6.1, assuming that only the reoxidation rate $k_{1b}$ is magnetic field dependent. Results are shown for the four experimental protocols described in the legend, with light switched on in the first 300 s, and off in the following 600 s. (b) The accumulated difference, calculated according to 6.3 for the three experimental protocols described in the legend.

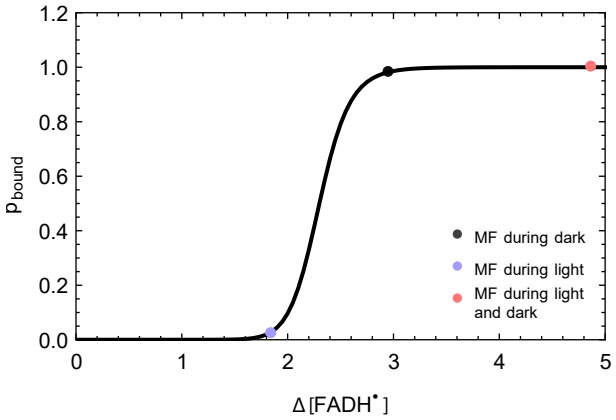


Figure 6.5: Phosphorylation binding curve with $t_{\text{L}} = 300$s, $t_{\text{D}} = 600$s, $k_{1b} = 10^{-3}$ s$^{-1}$, $k_1 = 4.8 \times 10^{-4}$ s$^{-1}$, the magnetic field only on the back reaction, and phosphorylation parameters described in the text.

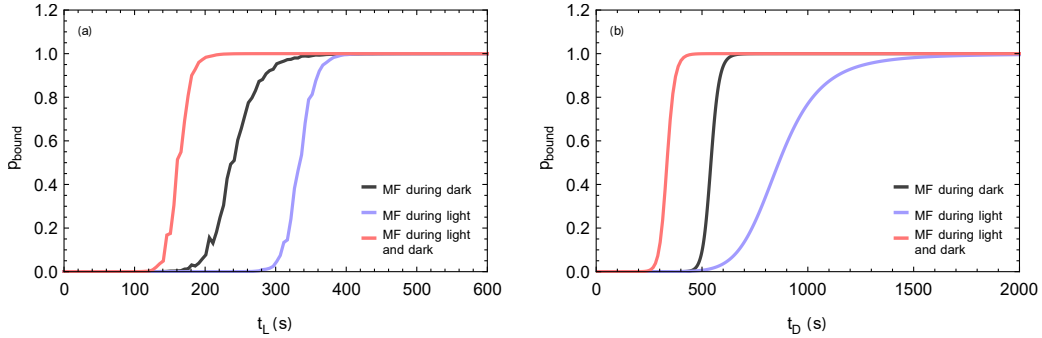


Figure 6.6: Phosphorylation binding as a function of $t_{\text{L}}$ and $t_{\text{D}}$ with $k_{1b} = 10^{-3}s^{-1}$, $k_1 = 4.8 \times 10^{-4}s^{-1}$. In fig (a) $t_{\text{D}} = 600s$ and in fig(b) $t_{\text{L}} = 300s$.

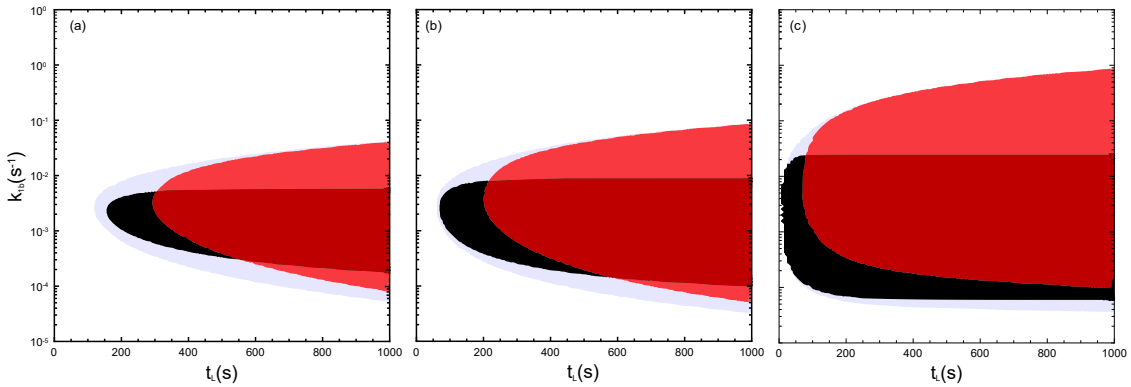


Figure 6.7: Phosphorylation binding for the three protocols, where black is the MF during the dark, red is the MF during the light, and blue is the MF during dark and light. The colored regions indicate where the phosphorylation is greater than 90%, and thus magnetic field effects are present. In each case, the dark period is fixed at 600s while the light period, and $k_{1b}$ are allowed to vary. Three cases for the rate $k_1$ are considered: (a) $k_1 = 4.8\times10^{-4}s^{-1}$, (b) $k_1 = 10^{-3}s^{-1}$, and (c) $k_1 = 10^{-2}s^{-1}$.

and allow both the reoxidation rate and light period to vary. The result of this is shown in Fig 6.7 where it can again be seen that a magnetic field effect is observed in all three protocols for a wide range of parameters.

Lastly, if we consider the case of allowing $t_D$ and $k_{1b}$ to vary, as in Fig. 6.8, we again see various regions emerge. In both situations, it appears that the MF during only the dark places the largest restriction on the available range of $k_{1b}$, which could prove to be useful to obtain this rate. There also exists a value of $k_{1b}$ above which no phosphorylation can occur, and depends on how the magnetic field is applied. For the parameters considered, varying $t_D$ depends sensitively on the values (note the difference in intensities considered between Fig. 6.7 and Fig. 6.8) chosen compared to $t_L$. Due to this, it may prove more useful to vary $t_L$, In addition, we see that there exists parameters that lead to a variety of the protocols being observable as before, but the details are more complicated. For example, in Fig. 6.8 (a) there is a region in which if there is a MFE observed for the MF during light only protocol, then there is necessarily a MFE for the other two as well. The conditions under which the MF during light only protocol leads to a MFE is much smaller compared to the other two protocols. This lends further support to the MF during the dark as being diagnostic, since

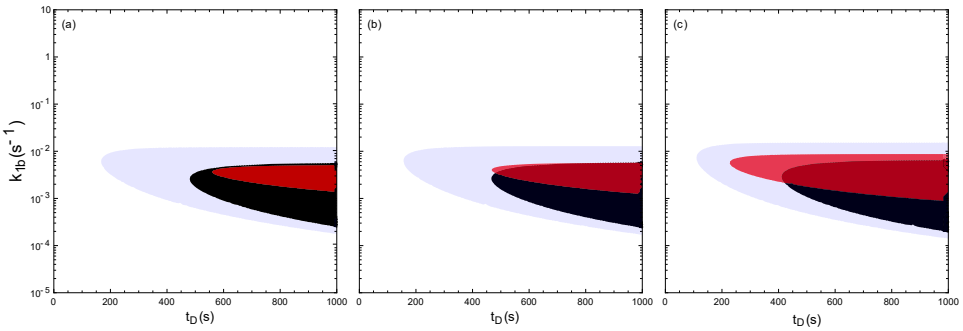


Figure 6.8: Phosphorylation binding for the three protocols, where black is the MF during the dark, red is the MF during the light, and blue is the MF during dark and light. The colored regions indicate where the phosphorylation is greater than 90%, and thus magnetic field effects are present. In each case, the light period is fixed at 300s while the dark period, and $k_{1b}$ are allowed to vary. Three cases for the rate $k_1$ are considered: (a) $k_1 = 4.8\times10^{-4}s^{-1}$, (b) $k_1 = 5.0 \times 10^{-4}s^{-1}$, and (c) $k_1 = 6 \times 10^{-4}s^{-1}$.

it is easier to realize experimentally as it occurs over a wider range of parameters.

However, this straightforward nature of the qualitative conclusions does not hold true if one applies magnetic field effects during the light cycle only. [35] In this condition, one might naively assume that observing magnetic field effects requires a magnetically sensitive step during the forward light reaction. Here we show that this is not the case. Rather, light can activate a population of semi-quinone states that can lead to magnetic field effects during reoxidation after the light is turned off, provided that the dark cycle is long enough so as to allow for these effects to accumulate sufficiently. Likewise, if the light period is long enough, sufficient reoxidation may occur during the light cycle so that magnetic field effects are observed when the magnetic field is applied during the light only. The dependence on the length of light and dark periods is strongly related to the dark reoxidation rate $k_{1b}$. It should be noted that using this rate in our model does not imply necessarily that a magnetically sensitive radical pair is formed during direct reoxidation from the Cry semiquinone state. Rather, $k_{1b}$ captures the combined rate of reoxidation through all channels from the Cry semiquinone state and could include scenarios where the majority of the Cry semiquinone population reoxidizes directly with no magnetic field effects and a smaller part of the Cry semiquinone population first is reduced fully and then reoxidizes with a strong magnetic field

effect. We investigated the relationship between $k_{1b}$ and the length of light and dark cycles in the three different experimental conditions. We found that there is generally a fairly sharp upper bound for $k_{1b}$ beyond which no magnetic field effects can be observed if the MF is applied only in the dark. This bound does not change significantly when light intensity is increased or the light or dark periods are lengthened. Similarly, the range of parameters for which magnetic field effects can be observed when the MF is only applied during light is narrowly bound by the $k_{1b}$ values. This means that one could use these two protocols to obtain information about $k_{1b}$ if it cannot be determined through more direct means.

## 6.3 Discussion

In this chapter we have presented model calculations that suggest a magnetic field effect when it is applied only during the light, in contrast with what was observed. The source of this inconsistency is due in part to the length of the light (and/or dark) time periods chosen. Furthermore, our calculations present a method of determining allowable reoxidation rates from experiments using alternating light and magnetic fields.

# Bibliography


[1] M. Ahmad and A. R. Cashmore. Hy4 gene of a. thaliana encodes a protein with characteristics of a blue-light photoreceptor. *Nature*, 366(6451):162–166, Nov 1993.

[2] M. Ahmad, P. Galland, T. Ritz, R. Wiltschko, and W. Wiltschko. Magnetic intensity affects cryptochrome-dependent responses in arabidopsis thaliana. *Planta*, 225(3):615–624, Feb 2007.

[3] M. Ahmad, N. Grancher, M. Heil, R. C. Black, B. Giovani, P. Galland, and D. Lardemer. Action spectrum for cryptochrome-dependent hypocotyl growth inhibition in arabidopsis. *Plant Physiology*, 129(2):774–785, June 2002.

[4] M. Ahmad, J. A. Jarillo, O. Smirnova, and A. R. Cashmore. The cry1 blue light photoreceptor of arabidopsis interacts with phytochrome a in vitro. *Molecular Cell*, 1(7):939–948, 1998.

[5] M. Ahmad, J. A. Jarillo, O. Smirnova, and A. R. Cashmore. The cry1 blue light photoreceptor of arabidopsis interacts with phytochrome a in vitro. *Molecular Cell*, 1(7):939–948, 1998.

[6] T. Alerstam. Flight by night or day? optimal daily timing of bird migration. *Journal of Theoretical Biology*, 258(4):530–536, 2009.

[7] C. Atkins, K. Bajpai, J. Rumball, and D. R. Kattnig. On the optimal relative orientation of radicals in the cryptochrome magnetic compass. *The Journal of Chemical Physics*, 151(6):065103, 2019.

[8] C. Aubert, M. H. Vos, P. Mathis, A. P. M. Eker, and K. Brettel. Intraprotein radical transfer during photoactivation of DNA photolyase. *Nature*, 405(6786):586–590, June 2000.

[9] N. S. Babcock and D. R. Kattnig. Electron-electron dipolar interaction poses a challenge to the radical pair mechanism of magnetoreception. *The journal of physical chemistry letters*, 11(7):2414–2421, Apr 2020. 32141754[pmid].

[10] R. Banerjee, E. Schleicher, S. Meier, R. M. Viana, R. Pokorny, M. Ahmad, R. Bittl, and A. Batschauer. The signaling state of arabidopsis cryptochrome 2 contains flavin semiquinone. *Journal of Biological Chemistry*, 282(20):14916–14922, May 2007.

[11] P. Berthold, E. Gwinner, and E. Sonnenschein. *Avian migration*. Springer Science & Business Media, 2013.

[12] T. Biskup, E. Schleicher, A. Okafuji, G. Link, K. Hitomi, E. D. Getzoff, and S. Weber. Direct observation of a photoinduced radical pair in a cryptochrome blue-light photoreceptor. *Angewandte Chemie International Edition*, 48(2):404–407, 2009.

[13] R. Blakemore. Magnetotactic bacteria. *Science*, 190(4212):377–379, 1975.

[14] J. R. Bolton and J. A. Weil. *Electron Paramagnetic Resonance*. John Wiley & Sons, Ltd, 2006.

[15] J.-P. Bouly, E. Schleicher, M. Dionisio-Sese, F. Vandenbussche, D. V. D. Straeten, N. Bakrim, S. Meier, A. Batschauer, P. Galland, R. Bittl, and M. Ahmad. Cryptochrome blue light photoreceptors are activated through interconversion of flavin redox states. *Journal of Biological Chemistry*, 282(13):9383–9391, Mar. 2007.

[16] B. Brocklehurst. Spin correlation in the geminate recombination of radical ions in hydrocarbons. part 1.—theory of the magnetic field effect. *J. Chem. Soc., Faraday Trans. 2*, 72:1869–1884, 1976.

[17] J. Cai, F. Caruso, and M. B. Plenio. Quantum limits for the magnetic sensitivity of a chemical compass. *Phys. Rev. A*, 85:040304, Apr 2012.

[18] F. Caruso, A. W. Chin, A. Datta, S. F. Huelga, and M. B. Plenio. Highly efficient energy excitation transfer in light-harvesting complexes: The fundamental role of noise-assisted transport. *The Journal of Chemical Physics*, 131(10):105106, 2009.

[19] A. R. Cashmore, J. A. Jarillo, Y.-J. Wu, and D. Liu. Cryptochromes: Blue light receptors for plants and animals. *Science*, 284(5415):760–765, 1999.

[20] I. Chaves, R. Pokorny, M. Byrdin, N. Hoang, T. Ritz, K. Brettel, L.-O. Essen, G. T. J. van der Horst, A. Batschauer, and M. Ahmad. The cryptochromes: Blue light photoreceptors in plants and animals. *Annual Review of Plant Biology*, 62(1):335–364, 2011. PMID: 21526969.

[21] S.-Y. Choi, B. Borghuis, R. Rea, E. S. Levitan, P. Sterling, and R. H. Kramer. Encoding light intensity by the cone photoreceptor synapse. *Neuron*, 48(4):555–562, 2005.

[22] F. Cintolesi, T. Ritz, C. Kay, C. Timmel, and P. Hore. Anisotropic recombination of an immobilized photoinduced radical pair in a 50-$\mu$T magnetic field: a model avian photomagnetoreceptor. *Chemical Physics*, 294(3):385–399, 2003. Structure-Mechanism in Photosynthesis Dedicated to the Memory of Professor Arnold Jan Hoff.

[23] G. L. Closs. Mechanism explaining nuclear spin polarizations in radical combination reactions. *Journal of the American Chemical Society*, 91(16):4552–4554, July 1969.

[24] O. Efimova and P. J. Hore. Role of exchange and dipolar interactions in the radical pair model of the avian magnetic compass. *Biophysical Journal*, 94(5):1565–1574, 2017/12/07 2008.

[25] A. Einwich, K. Dedek, P. K. Seth, S. Laubinger, and H. Mouritsen. A novel isoform of cryptochrome 4 (cry4b) is expressed in the retina of a night-migratory songbird. *Scientific Reports*, 10(1):15794, Sep 2020.

[26] S. T. Emlen. Migratory orientation in the indigo bunting, passerina cyanea: Part i: Evidence for use of celestial cues. *The Auk*, 84(3):309–342, 1967.

[27] S. T. Emlen. Migratory orientation in the indigo bunting, passerina cyanea. part ii: Mechanism of celestial orientation. *The Auk*, 84(4):463–489, 1967.

[28] E. W. Evans, D. R. Kattnig, K. B. Henbest, P. J. Hore, S. R. Mackenzie, and C. R. Timmel. Sub-millitesla magnetic field effects on the recombination reaction of flavin and ascorbic acid radicals. *The Journal of Chemical Physics*, 145(8):085101, 2016.

[29] M. V. Fedin, P. A. Purtov, and E. G. Bagryanskaya. Spin relaxation of radicals in low and zero magnetic field. *The Journal of Chemical Physics*, 118(1):192–201, 2003.

[30] R. J. Gegear, A. Casselman, S. Waddell, and S. M. Reppert. Cryptochrome mediates light-dependent magnetosensitivity in drosophila. *Nature*, 454(7207):1014–1018, July 2008.

[31] B. Giovani, M. Byrdin, M. Ahmad, and K. Brettel. Light-induced electron transfer in a cryptochrome blue-light photoreceptor. *Nature Structural & Molecular Biology*, 10(6):489–490, Jun 2003.

[32] E. Griffin, D. Staknis, and C. Weitz. Light-independent role of cry1 and cry2 in the mammalian circadian clock. *SCIENCE*, 286(5440):768–771, OCT 22 1999.

[33] A. Günther, A. Einwich, E. Sjulstok, R. Feederle, P. Bolte, K.-W. Koch, I. A. Solov'yov, and H. Mouritsen. Double-cone localization and seasonal expression pattern suggest a role in magnetoreception for european robin cryptochrome 4. *Current Biology*, 28(2):211–223.e4, 2018.

[34] R. Haberkorn. Density matrix description of spin-selective radical pair reactions. *Molecular Physics*, 32(5):1491–1493, 1976.

[35] M. Hammad, M. Albaqami, M. Pooam, E. Kernevez, J. Witczak, T. Ritz, C. Martino, and M. Ahmad. Cryptochrome mediated magnetic sensitivity in arabidopsis occurs independently of light-induced electron transfer to the flavin. *Photochemical & Photobiological Sciences*, 19, 02 2020.

[36] K. B. Henbest, K. Maeda, P. J. Hore, M. Joshi, A. Bacher, R. Bittl, S. Weber, C. R. Timmel, and E. Schleicher. Magnetic-field effect on the photoactivation reaction of ¡i¿escherichia coli¡/i¿ dna photolyase. *Proceedings of the National Academy of Sciences*, 105(38):14395–14399, 2008.

[37] D. Heyers, M. Manns, H. Luksch, O. Güntürkün, and H. Mouritsen. A visual pathway links brain structures active during magnetic compass orientation in migratory birds. *PLOS ONE*, 2:1–6, 09 2007.

[38] E. Hill and T. Ritz. Can disordered radical pair systems provide a basis for a agnetic compass in animals? *J R Soc Interface*, 7 Suppl 2(Suppl 2):S265–71, Nov. 2009.

[39] H. G. Hiscock, T. W. Hiscock, D. R. Kattnig, T. Scrivener, A. M. Lewis, D. E. Manolopoulos, and P. J. Hore. Navigating at night: fundamental limits on the sensitivity of radical pair magnetoreception under dim light. *Quarterly Reviews of Biophysics*, 52:e9, 2019.

[40] H. G. Hiscock, H. Mouritsen, D. E. Manolopoulos, and P. Hore. Disruption of magnetic compass orientation in migratory birds by radiofrequency electromagnetic fields. *Biophysical Journal*, 113(7):1475–1484, 2017.

[41] H. G. Hiscock, S. Worster, D. R. Kattnig, C. Steers, Y. Jin, D. E. Manolopoulos, H. Mouritsen, and P. J. Hore. The quantum needle of the avian magnetic compass. *Proceedings of the National Academyf of Sciences*, 113(17):4634–4639, 2016.

[42] T. Hochstoeger, T. A. Said, D. Maestre, F. Walter, A. Vilceanu, M. Pedron, T. D. Cushion, W. Snider, S. Nimpf, G. C. Nordmann, L. Landler, N. Edelman, L. Kruppa, G. Dürnberger, K. Mechtler, S. Schuechner, E. Ogris, E. P. Malkemper, S. Weber, E. Schleicher, and D. A. Keays. The biophysical, molecular, and anatomical landscape of pigeon CRY4: A candidate light-based quantal magnetosensor. *Science Advances*, 6(33), Aug. 2020.

[43] H. J. Hogben, T. Biskup, and P. J. Hore. Entanglement and sources of magnetic anisotropy in radical pair-based avian magnetoreceptors. *Phys. Rev. Lett.*, 109:220501, Nov 2012.

[44] H. J. Hogben, O. Efimova, N. Wagner-Rundell, C. R. Timmel, and P. Hore. Possible involvement of superoxide and dioxygen with cryptochrome in avian magnetoreception: Origin of zeeman resonances observed by in vivo epr spectroscopy. *Chemical Physics Letters*, 480(1):118 – 122, 2009.

[45] F. T. HONG. Photoelectric and magneto-orientation effects in pigmented biological membranes. In M. Kerker, A. C. Zettlemoyer, and R. L. Rowell, editors, *Plenary and Invited Lectures*, pages 497–523. Academic Press, 1977.

[46] F. T. Hong. Magnetic field effects on biomolecules, cells, and living organisms. *Biosystems.*, 36(3):187–229, 1995.

[47] P. J. Hore and H. Mouritsen. The radical-pair mechanism of magnetoreception. *Annual Review of Biophysics*, 45(1):299–344, 2016. PMID: 27216936.

[48] J. D. Jackson. *Classical electrodynamics*. Wiley, New York, NY, 3rd ed. edition, 1999.

[49] S. Johnsen and K. Lohmann. Magnetoreception in animals. *Physics Today - PHYS TODAY*, 61, 03 2008.

[50] R. Kaptein and J. Oosterhoff. Chemically induced dynamic nuclear polarization II. *Chemical Physics Letters*, 4(4):195–197, Nov. 1969.

[51] D. R. Kattnig and P. J. Hore. The sensitivity of a radical pair compass magnetoreceptor can be significantly amplified by radical scavengers. *Scientific Reports*, 7(1):11640, Sep 2017.

[52] D. R. Kattnig, I. A. Solov'yov, and P. J. Hore. Electron spin relaxation in cryptochrome-based magnetoreception. *Phys. Chem. Chem. Phys.*, 18:12443–12456, 2016.

[53] N. Keary, T. Ruploh, J. Voss, P. Thalau, R. Wiltschko, W. Wiltschko, and H.-J. Bischof. Oscillating magnetic field disrupts magnetic orientation in zebra finches, taeniopygia guttata. *Frontiers in Zoology*, 6(1):25, Oct 2009.

[54] R. Kendrick and G. Kronenberg. *Photomorphogenesis in Plants*. Springer Netherlands, Reading, Massachusetts, 1994.

[55] C. Kerpal, S. Richert, J. G. Storey, S. Pillai, P. A. Liddell, D. Gust, S. R. Mackenzie, P. J. Hore, and C. R. Timmel. Chemical compass behaviour at microtesla magnetic fields strengthens the radical pair hypothesis of avian magnetoreception. *Nature Communications*, 10(1):3707, Aug 2019.

[56] T. Kimchi, A. S. Etienne, and J. Terkel. A subterranean mammal uses the magnetic compass for path integration. *Proceedings of the National Academy of Sciences*, 101(4):1105–1109, 2004.

[57] J. L. Kirschvink and J. L. Gould. Biogenic magnetite as a basis for magnetic field detection in animals. *Biosystems*, 13(3):181–201, 1981.

[58] R. H. G. Klaassen, M. Hake, R. Strandberg, B. J. Koks, C. Trierweiler, K.-M. Exo, F. Bairlein, and T. Alerstam. When and where does mortality occur in migratory birds? direct evidence from long-term satellite tracking of raptors. *Journal of Animal Ecology*, 83(1):176–184, 2014.

[59] T. Kottke, A. Batschauer, M. Ahmad, and J. Heberle. Blue-light-induced changes in arabidopsis cryptochrome 1 probed by FTIR difference spectroscopy. *Biochemistry*, 45(8):2472–2479, Feb. 2006.

[60] G. Kramer. Experiments on bird orientation. *Ibis*, 94(2):265–285, 1952.

[61] R. Kubo. *A Stochastic Theory of Line Shape*, pages 101–127. John Wiley & Sons, Ltd, 1969.

[62] K. Kume, M. Zylka, S. Sriram, L. Shearman, D. Weaver, X. Jin, E. Maywood, M. Hastings, and S. Reppert. mcry1 and mcry2 are essential components of the negative limb of the circadian clock feedback loop. *CELL*, 98(2):193–205, JUL 23 1999.

[63] R. J. Kutta, N. Archipowa, L. O. Johannissen, A. R. Jones, and N. S. Scrutton. Vertebrate cryptochromes are vestigial flavoproteins. *Scientific reports*, 7:44906–44906, Mar 2017.

[64] N. Lambert, S. D. Liberato, C. Emary, and F. Nori. Radical-pair model of magnetoreception with spin–orbit coupling. *New Journal of Physics*, 15(8):083024, aug 2013.

[65] J. C. S. Lau, N. Wagner-Rundell, C. T. Rodgers, N. J. B. Green, and P. J. Hore. Effects of disorder and motion in a radical pair magnetoreceptor. *Journal of The Royal Society Interface*, 7(suppl_2):S257–S264, 2009.

[66] M. J. M. Leask. A physicochemical mechanism for magnetic field detection by migratory birds and homing pigeons. *Nature*, 267(5607):144–145, May 1977.

[67] B. Leberecht, D. Kobylkov, T. Karwinkel, S. Döge, L. Burnus, S. Y. Wong, S. Apte, K. Haase, I. Musielak, R. Chetverikova, G. Dautaj, M. Bassetto, M. Winklhofer, P. J. Hore, and H. Mouritsen. Broadband 75–85 mhz radiofrequency fields disrupt magnetic compass orientation in night-migratory songbirds consistent with a flavin-based radical pair magnetoreceptor. *Journal of Comparative Physiology A*, 208(1):97–106, Jan 2022.

[68] A. A. Lee, J. C. S. Lau, H. J. Hogben, T. Biskup, D. R. Kattnig, and P. J. Hore. Alternative radical pairs for cryptochrome-based magnetoreception. *Journal of The Royal Society Interface*, 11(95):20131063, 2014.

[69] Q.-H. Li and H.-Q. Yang. Cryptochrome signaling in plants†. *Photochemistry and Photobiology*, 83(1):94–101, 2007.

[70] M. Liedvogel, K. Maeda, K. Henbest, E. Schleicher, T. Simon, C. R. Timmel, P. J. Hore, and H. Mouritsen. Chemical magnetoreception: Bird cryptochrome 1a is excited by blue light and forms long-lived radical-pairs. *PLoS ONE*, 2(10):e1106, Oct. 2007.

[71] C. Lin, D. E. Robertson, M. Ahmad, A. A. Raibekas, M. S. Jorns, P. L. Dutton, and A. R. Cashmore. Association of flavin adenine dinucleotide with the arabidopsis blue light receptor cry1. *Science*, 269(5226):968–970, Aug. 1995.

[72] C. Lin and T. Todo. The cryptochromes. *Genome Biology*, 6(5):220, Apr 2005.

[73] K. J. Lohmann. Magnetic-field perception. *Nature*, 464(7292):1140–1142, Apr. 2010.

[74] K. J. Lohmann, S. D. Cain, S. A. Dodge, and C. M. F. Lohmann. Regional magnetic fields as navigational markers for sea turtles. *Science*, 294(5541):364–366, 2001.

[75] K. J. Lohmann, C. M. F. Lohmann, L. M. Ehrhart, D. A. Bagley, and T. Swing. Geomagnetic map used in sea-turtle navigation. *Nature*, 428(6986):909–910, Apr 2004.

[76] K. J. Lohmann, C. M. F. Lohmann, and N. F. Putman. Magnetic maps in animals: nature's GPS. *Journal of Experimental Biology*, 210(21):3697–3705, 11 2007.

[77] K. Maeda, K. B. Henbest, F. Cintolesi, I. Kuprov, C. T. Rodgers, P. A. Liddell, D. Gust, C. R. Timmel, and P. J. Hore. Chemical compass model of avian magnetoreception. *Nature*, 453(7193):387–390, May 2008.

[78] K. Maeda, A. J. Robinson, K. B. Henbest, H. J. Hogben, T. Biskup, M. Ahmad, E. Schleicher, S. Weber, C. R. Timmel, and P. J. Hore. Magnetically sensitive light-induced reactions in cryptochrome are consistent with its proposed role as a magnetoreceptor. *Proceedings of the National Academy of Sciences*, 109(13):4774–4779, 2012.

[79] K. Malhotra, S.-T. Kim, A. Batschauer, L. Dawut, and A. Sancar. Putative blue-light photoreceptors from arabidopsis thaliana and sinapis alba with a high degree of sequence homology to dna photolyase contain the two photolyase cofactors but lack dna repair activity. *Biochemistry*, 34(20):6892–6899, May 1995.

[80] A. Möller, S. Sagasser, W. Wiltschko, and B. Schierwater. Retinal cryptochrome in a migratory passerine bird: a possible transducer for the avian magnetic compass. *Naturwissenschaften*, 91(12):585–588, Dec 2004.

[81] D. Moore. Kinetic treatment of photochemical reactions. *International Journal of Pharmaceutics*, 63(1):R5–R7, Aug. 1990.

[82] H. Mouritsen. Long-distance navigation and magnetoreception in migratory animals. *Nature*, 558(7708):50–59, Jun 2018.

[83] H. Mouritsen, G. Feenders, M. Liedvogel, K. Wada, and E. D. Jarvis. Night-vision brain area in migratory songbirds. *Proceedings of the National Academy of Sciences*, 102(23):8339–8344, 2005.

[84] H. Mouritsen, U. Janssen-Bienhold, M. Liedvogel, G. Feenders, J. Stalleicken, P. Dirks, and R. Weiler. Cryptochromes and neuronal-activity markers colocalize in the retina of migratory birds during magnetic orientation. *Proceedings of the National Academy of Sciences*, 101(39):14294–14299, 2004.

[85] R. Muheim, J. Bäckman, and S. Åkesson. Magnetic compass orientation in european robins is dependent on both wavelength and intensity of light. *Journal of Experimental Biology*, 205(24):3845–3856, 12 2002.

[86] P. Müller and J.-P. Bouly. Searching for the mechanism of signalling by plant photoreceptor cryptochrome. *FEBS Letters*, 589(2):189–192, Dec. 2014.

[87] P. Müller, J. Yamamoto, R. Martin, S. Iwai, and K. Brettel. Discovery and functional analysis of a 4th electron-transferring tryptophan conserved exclusively in animal cryptochromes and (6-4) photolyases. *Chemical Communications*, 51(85):15502–15505, 2015.

[88] U. Munro, J. A. Munro, J. B. Phillips, R. Wiltschko, and W. Wiltschko. Evidence for a magnetite-based navigational "map" in birds. *Naturwissenschaften*, 84(1):26–28, Jan 1997.

[89] P. Müller and M. Ahmad. Light-activated cryptochrome reacts with molecular oxygen to form a flavin–superoxide radical pair consistent with magnetoreception*. *Journal of Biological Chemistry*, 286(24):21033–21040, 2011.

[90] L. C. Naisbett-Jones, N. F. Putman, J. F. Stephenson, S. Ladak, and K. A. Young. A magnetic map leads juvenile european eels to the gulf stream. *Current Biology*, 27(8):1236–1240, 2017.

[91] C. Nießner, S. Denzau, J. C. Gross, L. Peichl, H.-J. Bischof, G. Fleissner, W. Wiltschko, and R. Wiltschko. Avian ultraviolet/violet cones identified as probable magnetoreceptors. *PLoS ONE*, 6(5):e20091, May 2011.

[92] C. Nießner, S. Denzau, L. Peichl, W. Wiltschko, and R. Wiltschko. Magnetoreception: activation of avian cryptochrome 1a in various light conditions. *Journal of Comparative Physiology A*, 204(12):977–984, Dec 2018.

[93] C. Nießner, S. Denzau, K. Stapput, M. Ahmad, L. Peichl, W. Wiltschko, and R. Wiltschko. Magnetoreception: activated cryptochrome 1a concurs with magnetic orientation in birds. *Journal of The Royal Society Interface*, 10(88):20130638, 2013.

[94] D. Nohr, S. Franz, R. Rodriguez, B. Paulus, L.-O. Essen, S. Weber, and E. Schleicher. Extended electron-transfer in animal cryptochromes mediated by a tetrad of aromatic amino acids. *Biophysical Journal*, 111(2):301–311, July 2016.

[95] N. Ozturk, C. P. Selby, S.-H. Song, R. Ye, C. Tan, Y.-T. Kao, D. Zhong, and A. Sancar. Comparative photochemistry of animal type 1 and type 4 cryptochromes. *Biochemistry*, 48(36):8585–8593, Aug. 2009.

[96] C. L. Partch, M. W. Clarkson, S. Özgür, A. L. Lee, and A. Sancar. Role of structural plasticity in signal transduction by the cryptochrome blue-light photoreceptor. *Biochemistry*, 44(10):3795–3805, Mar 2005.

[97] J. B. Pedersen, C. Nielsen, and I. A. Solov'yov. Multiscale description of avian migration: from chemical compass to behaviour modeling. *Scientific reports*, 6:36709, November 2016.

[98] J. Phillips, R. Muheim, M. Painter, J. Raines, C. Anderson, L. Landler, D. Dommer, A. Raines, M. Deutschlander, J. Whitehead, N. E. Fitzpatrick, P. Youmans, C. Borland, K. Sloan, and K. McKenna. Why is it so difficult to study magnetic compass orientation in murine rodents? *Journal of Comparative Physiology A*, 208(1):197–212, Jan 2022.

[99] J. B. Phillips. Two magnetoreception pathways in a migratory salamander. *Science*, 233(4765):765–767, 1986.

[100] A. Pinzon-Rodriguez, S. Bensch, and R. Muheim. Expression patterns of cryptochrome genes in avian retina suggest involvement of cry4 in light-dependent magnetoreception. *Journal of The Royal Society Interface*, 15(140):20180058, 2018.

[101] M. B. Plenio and S. F. Huelga. Dephasing-assisted transport: quantum networks and biomolecules. *New Journal of Physics*, 10(11):113019, 2008.

[102] P. Plötz, M. Lubasch, and S. Wimberger. Detection of avoided crossings by fidelity. *Physica A: Statistical Mechanics and its Applications*, 390(7):1363–1369, 2011.

[103] J. Ponnu and U. Hoecker. Signaling mechanisms by arabidopsis cryptochromes. *Frontiers in Plant Science*, 13, 2022.

[104] M. Pooam, L.-D. Arthaut, D. Burdick, J. Link, C. F. Martino, and M. Ahmad. Magnetic sensitivity mediated by the arabidopsis blue-light receptor cryptochrome occurs during flavin reoxidation in the dark. *Planta*, 249(2):319–332, Feb 2019.

[105] M. Procopio, J. Link, D. Engle, J. Witczak, T. Ritz, and M. Ahmad. Kinetic modeling of the arabidopsis cryptochrome photocycle: Fadho accumulation correlates with biological activity. *Frontiers in Plant Science*, 7, 2016.

[106] M. Procopio and T. Ritz. Inhomogeneous ensembles of radical pairs in chemical compasses. *Scientific Reports*, 6(1):35443, Nov 2016.

[107] M. Procopio and T. Ritz. The reference-probe model for a robust and optimal radical-pair-based magnetic compass sensor. *The Journal of Chemical Physics*, 152(6):065104, 2020.

[108] N. Putman, C. Endres, C. Lohmann, and K. Lohmann. Longitude perception and bicoordinate magnetic maps in sea turtles. *Current Biology*, 21(6):463–466, 2011.

[109] Y. Ren, H. G. Hiscock, and P. Hore. Angular precision of radical pair compass magnetoreceptors. *Biophysical Journal*, 120(3):547–555, 2021.

[110] T. Ritz, S. Adem, and K. Schulten. A model for photoreceptor-based magnetoreception in birds. *Biophysical Journal*, 78(2):707–718, 2017/12/07 2000.

[111] T. Ritz, M. Ahmad, H. Mouritsen, R. Wiltschko, and W. Wiltschko. Photoreceptor-based magnetoreception: optimal design of receptor molecules, cells, and neuronal processing. *Journal of The Royal Society Interface*, 7(suppl_2):S135–S146, 2010.

[112] T. Ritz, P. Thalau, J. B. Phillips, R. Wiltschko, and W. Wiltschko. Resonance effects indicate a radical-pair mechanism for avian magnetic compass. *Nature*, 429(6988):177–180, May 2004.

[113] T. Ritz, R. Wiltschko, P. J. Hore, C. T. Rodgers, K. Stapput, P. Thalau, C. R. Timmel, and W. Wiltschko. Magnetic compass of birds is based on a molecule with optimal directional sensitivity. *Biophysical journal*, 96(8):3451–3457, Apr 2009.

[114] J. J. Sakurai and J. Napolitano. *Modern Quantum Mechanics*. Addison-Wesley, 2011.

[115] A. Sancar. Structure and function of photolyase and in vivo enzymology: 50th anniversary. *Journal of Biological Chemistry*, 283(47):32153–32157, Nov. 2008.

[116] K. Schulten, C. E. Swenberg, and A. Weller. A biomagnetic sensory mechanism based on magnetic field modulated coherent electron spin motion. *Zeitschrift für Physikalische Chemie*, 111(1):1–5, 1978.

[117] K. Schulten and A. Windemuth. Model for a physiological magnetic compass. *Biophysical Effects of Steady Magnetic Fields*, 01 1986.

[118] K. Schulten and P. G. Wolynes. Semiclassical description of electron spin motion in radicals including the effect of electron hopping. *The Journal of Chemical Physics*, 68(7):3292–3297, 1978.

[119] D. Shalitin, H. Yang, T. C. Mockler, M. Maymon, H. Guo, G. C. Whitelam, and C. Lin. Regulation of arabidopsis cryptochrome 2 by blue-light-dependent phosphorylation. *Nature*, 417(6890):763–767, Jun 2002.

[120] D. Shalitin, X. Yu, M. Maymon, T. Mockler, and C. Lin. Blue Light–Dependent in Vivo and in Vitro Phosphorylation of Arabidopsis Cryptochrome 1 . *The Plant Cell*, 15(10):2421–2429, 10 2003.

[121] D. M. W. Sheppard, J. Li, K. B. Henbest, S. R. T. Neil, K. Maeda, J. Storey, E. Schleicher, T. Biskup, R. Rodriguez, S. Weber, P. J. Hore, C. R. Timmel, and S. R. Mackenzie. Millitesla magnetic field effects on the photocycle of an animal cryptochrome. *Scientific reports*, 7:42228–42228, Feb 2017.

[122] C. Smith. *Biology of Sensory Systems*. John Wiley & Sons, Ltd, 2nd ed. edition, 2009.

[123] I. A. Solov'yov, D. E. Chandler, and K. Schulten. Magnetic field effects in arabidopsis thaliana cryptochrome-1. *Biophysical Journal*, 92(8):2711 – 2726, 2007.

[124] I. A. Solov'yov and K. Schulten. Magnetoreception through cryptochrome may involve superoxide. *Biophysical Journal*, 96(12):4804 – 4813, 2009.

[125] K. Stapput, P. Thalau, R. Wiltschko, and W. Wiltschko. Orientation of birds in total darkness. *Current Biology*, 18(8):602–606, 2008.

[126] D. Stass, J. Woodward, C. Timmel, P. Hore, and K. McLauchlan. Radiofrequency magnetic field effects on chemical reaction yields. *Chemical Physics Letters*, 329(1):15–22, 2000.

[127] U. E. Steiner and T. Ulrich. Magnetic field effects in chemical kinetics and related phenomena. *Chemical Reviews*, 89(1):51–147, 1989.

[128] A. M. Stoneham, E. M. Gauger, K. Porfyrakis, S. C. Benjamin, and B. W. Lovett. A new type of radical-pair-based model for magnetoreception. *Biophysical Journal*, 102(5):961–968, Mar. 2012.

[129] R. Storn and K. Price. Differential evolution: A simple and efficient heuristic for global optimization over continuous spaces. *Journal of Global Optimization*, 11(4):341–359, Dec 1997.

[130] J. M. T. Thompson, C. R. Timmel, and K. B. Henbest. A study of spin chemistry in weak magnetic fields. *Philosophical Transactions of the Royal Society of London. Series A: Mathematical, Physical and Engineering Sciences*, 362(1825):2573–2589, 2004.

[131] C. Timmel and P. Hore. Oscillating magnetic field effects on the yields of radical pair reactions. *Chemical Physics Letters*, 257(3):401–408, 1996.

[132] C. Timmel, U. Till, B. Brocklehurst, K. Mclauchlan, and P. Hore. Effects of weak magnetic fields on free radical recombination reactions. *Molecular Physics*, 95(1):71–89, 1998.

[133] C. R. Timmel, F. Cintolesi, B. Brocklehurst, and P. J. Hore. Model calculations of magnetic field effects on the recombination reactions of radicals with anisotropic hyperfine interactions. *Chemical Physics Letters*, 334(4):387–395, Feb 2001.

[134] M. Vácha, T. Pužová, and M. Kvíćalová. Radio frequency magnetic fields disrupt magnetoreception in American cockroach. *Journal of Experimental Biology*, 212(21):3473–3477, 11 2009.

[135] G. van der Horst, M. Muijtjens, K. Kobayashi, R. Takano, S. Kanno, M. Takao, J. de Wit, A. Verkerk, A. Eker, D. van Leenen, R. Buijs, D. Bootsma, J. Hoeijmakers, and A. Yasui. Mammalian cry1 and cry2 are essential for maintenance of circadian rhythms. *NATURE*, 398(6728):627–630, APR 15 1999.

[136] J. Vanderstraeten, P. Gailly, and E. P. Malkemper. Low-light dependence of the magnetic field effect on cryptochromes: Possible relevance to plant ecology. *Frontiers in Plant Science*, 9, 2018.

[137] P. Virtanen, R. Gommers, T. E. Oliphant, M. Haberland, T. Reddy, D. Cournapeau, E. Burovski, P. Peterson, W. Weckesser, J. Bright, S. J. van der Walt, M. Brett, J. Wilson, K. J. Millman, N. Mayorov, A. R. J. Nelson, E. Jones, R. Kern, E. Larson, C. J. Carey, İ. Polat, Y. Feng, E. W. Moore, J. VanderPlas, D. Laxalde, J. Perktold, R. Cimrman, I. Henriksen, E. A. Quintero, C. R. Harris, A. M. Archibald, A. H. Ribeiro, F. Pedregosa, P. van Mulbregt, and SciPy 1.0 Contributors. SciPy 1.0: Fundamental Algorithms for Scientific Computing in Python. *Nature Methods*, 17:261–272, 2020.

[138] C. Walcott. Magnetic orientation in homing pigeons. *IEEE Transactions on Magnetics*, 16(5):1008–1013, 1980.

[139] R. Watari, C. Yamaguchi, W. Zemba, Y. Kubo, K. Okano, and T. Okano. Light-dependent structural change of chicken retinal cryptochrome4 *. *Journal of Biological Chemistry*, 287(51):42634–42641, Dec 2012.

[140] J. C. Weaver, T. E. Vaughan, and R. D. Astumian. Biological sensing of small field differences by magnetically sensitive chemical reactions. *Nature*, 405(6787):707–709, 2000.

[141] S. Weber. Light-driven enzymatic catalysis of DNA repair: a review of recent biophysical studies on photolyase. *Biochimica et Biophysica Acta (BBA) - Bioenergetics*, 1707(1):1–23, Feb. 2005.

[142] R. Wiltschko, M. Ahmad, C. Nießner, D. Gehring, and W. Wiltschko. Light-dependent magnetoreception in birds: the crucial step occurs in the dark. *Journal of The Royal Society Interface*, 13(118):20151010, 2016.

[143] R. Wiltschko, C. Nießner, and W. Wiltschko. The magnetic compass of birds: The role of cryptochrome. *Frontiers in Physiology*, 12, 05 2021.

[144] R. Wiltschko, K. Stapput, P. Thalau, and W. Wiltschko. Directional orientation of birds by the magnetic field under different light conditions. *Journal of The Royal Society Interface*, 7(suppl_2):S163–S177, 2010.

[145] R. Wiltschko, P. Thalau, D. Gehring, C. Nießner, T. Ritz, and W. Wiltschko. Magnetoreception in birds: the effect of radio-frequency fields. *Journal of The Royal Society Interface*, 12(103):20141103, 2015.

[146] R. Wiltschko and W. Wiltschko. Magnetoreception in birds. *Journal of The Royal Society Interface*, 16(158):20190295, 2019.

[147] R. Wiltschko and W. Wiltschko. The discovery of the use of magnetic navigational information. *Journal of Comparative Physiology A*, 208(1):9–18, Jan 2022.

[148] W. Wiltschko. Compasses used by birds. *Comparative Biochemistry and Physiology Part A: Physiology*, 76(4):709–717, 1983.

[149] W. Wiltschko, L. Dehe, K. Stapput, P. Thalau, and R. Wiltschko. Magnetoreception in birds: No intensity window in "fixed direction" responses. *Die Naturwissenschaften*, 97:37–42, 09 2009.

[150] W. Wiltschko, R. Freire, U. Munro, T. Ritz, L. Rogers, P. Thalau, and R. Wiltschko. The magnetic compass of domestic chickens, Gallus gallus. *Journal of Experimental Biology*, 210(13):2300–2310, 07 2007.

[151] W. Wiltschko, M. Gesson, and R. Wiltschko. Magnetic compass orientation of european robins under 565 nm green light. *Naturwissenschaften*, 88(9):387–390, Sep 2001.

[152] W. Wiltschko and F. W. Merkel. Orientierung zugunruhiger rotkehlchen im statischen magnetfeld. *Verh. Dtsch. Zool. Ges*, 59:362–367, 1966.

[153] W. Wiltschko, U. Munro, H. Ford, and R. Wiltschko. Magnetic orientation in birds: non-compass responses under monochromatic light of increased intensity. *Proceedings of the Royal Society of London. Series B: Biological Sciences*, 270(1529):2133–2140, 2003.

[154] W. Wiltschko and R. Wiltschko. Magnetic compass of european robins. *Science*, 176(4030):62–64, 1972.

[155] W. Wiltschko and R. Wiltschko. Disorientation of inexperienced young pigeons after transportation in total darkness. *Nature*, 291(5814):433–434, Jun 1981.

[156] W. Wiltschko and R. Wiltschko. Migratory orientation of european robins is affected by the wavelength of light as well as by a magnetic pulse. *Journal of Comparative Physiology A-Sensory Neural and Behavioral Physiology*, 177(3):363–369, SEP 1995.

[157] W. Wiltschko and R. Wiltschko. Light-dependent magnetoreception in birds: the behaviour of European robins, Erithacus rubecula, under monochromatic light of various wavelengths and intensities. *Journal of Experimental Biology*, 204(19):3295–3302, 10 2001.

[158] W. Wiltschko, R. Wiltschko, and U. Munro. Light-dependent magnetoreception in birds: Does directional information change with light intensity? *Naturwissenschaften*, 87(1):36–40, Jan 2000.

[159] W. Wiltschko, R. Wiltschko, and U. Munro. Light-dependent magnetoreception in birds: the effect of intensity of 565-nm green light. *Naturwissenschaften*, 87(8):366–369, Aug 2000.

[160] S. Y. Wong, Y. Wei, H. Mouritsen, I. A. Solov'yov, and P. J. Hore. Cryptochrome magnetoreception: four tryptophans could be better than three. *Journal of the Royal Society, Interface*, 18(184):20210601–20210601, Nov 2021. 34753309[pmid].

[161] J. Woodward, R. Jackson, C. Timmel, P. Hore, and K. McLauchlan. Resonant radiofrequency magnetic field effects on a chemical reaction. *Chemical Physics Letters*, 272(5):376–382, 1997.

[162] S. Worster, D. R. Kattnig, and P. J. Hore. Spin relaxation of radicals in cryptochrome and its role in avian magnetoreception. *The Journal of Chemical Physics*, 145(3):035104, 2016.

[163] S. Worster, H. Mouritsen, and P. J. Hore. A light-dependent magnetoreception mechanism insensitive to light intensity and polarization. *Journal of The Royal Society Interface*, 14(134):20170405, Sept. 2017.

[164] H. Wu, A. Scholten, A. Einwich, H. Mouritsen, and K.-W. Koch. Protein-protein interaction of the putative magnetoreceptor cryptochrome 4 expressed in the avian retina. *Scientific Reports*, 10(1):7364, Apr 2020.

[165] J. Xu, L. E. Jarocha, T. Zollitsch, M. Konowalczyk, K. B. Henbest, S. Richert, M. J. Golesworthy, J. Schmidt, V. Déjean, D. J. C. Sowood, M. Bassetto, J. Luo, J. R. Walton, J. Fleming, Y. Wei, T. L. Pitcher, G. Moise, M. Herrmann, H. Yin, H. Wu, R. Bartölke, S. J. Kä sehagen, S. Horst, G. Dautaj, P. D. F. Murton, A. S. Gehrckens, Y. Chelliah, J. S. Takahashi, K.-W. Koch, S. Weber, I. A. Solov'yov, C. Xie, S. R. Mackenzie, C. R. Timmel, H. Mouritsen, and P. J. Hore. Magnetic sensitivity of cryptochrome 4 from a migratory songbird. *Nature*, 594(7864):535–540, Jun 2021.

[166] M. Zapka, D. Heyers, M. Liedvogel, E. Jarvis, and H. Mouritsen. Night-time neuronal activation of cluster n in a day- and night-migrating songbird. *European Journal of Neuroscience*, 32(4):619–624, 2010.

[167] A. Zeugner, M. Byrdin, J.-P. Bouly, N. Bakrim, B. Giovani, K. Brettel, and M. Ahmad. Light-induced electron transfer in arabidopsis cryptochrome-1 correlates with in vivo function. *Journal of Biological Chemistry*, 280(20):19437–19440, 2005.

[168] B. D. Zoltowski, Y. Chelliah, A. Wickramaratne, L. Jarocha, N. Karki, W. Xu, H. Mouritsen, P. J. Hore, R. E. Hibbs, C. B. Green, and J. S. Takahashi. Chemical and structural analysis of a photoactive vertebrate cryptochrome from pigeon. *Proceedings of the National Academy of Sciences*, 116(39):19449–19457, 2019.

[169] B. D. Zoltowski and K. H. Gardner. Tripping the light fantastic: Blue-light photoreceptors as examples of environmentally modulated protein protein interactions. *Biochemistry*, 50(1):4–16, Jan 2011.